NPS-PH-92-002

NAVAL POSTGRADUATE SCHOOL

Monterey, California

ON THE USE OF SYMPATHETIC
RESONATORS TO IMPROVE LOW-FREQUENCY
UNDERWATER TRANSDUCER PERFORMANCE

S. R. BAKER AND J. M. ELLSWORTH

OCTOBER 1991

Technical Report

Prepared for: Naval Postgraduate School, Monterey, California 93943

NAVAL POSTGRADUATE SCHOOL
Monterey, California

Rear Admiral Ralph W. West, Jr.
Superintendent

Harrison Shull
Provost

The work reported herein was supported by the Naval Postgraduate School.

This report was prepared by:

STEVEN R. BAKER
Associate Professor of Physics

JOHN M. ELLSWORTH
LT, USN

Reviewed by:

KARLHEINZ E. WOEHLER
Chairman, Department of Physics

Released by:

PAUL J. MARTO
Dean of Research

28 Oct 1991
Date

REPORT DOCUMENTATION PAGE

Form Approved
OMB No. 0704-0188

1a REPORT SECURITY CLASSIFICATION UNCLASSIFIED	1b RESTRICTIVE MARKINGS
2a SECURITY CLASSIFICATION AUTHORITY	3 DISTRIBUTION/AVAILABILITY OF REPORT Approved for public release; distribution unlimited.
2b DECLASSIFICATION/DOWNGRADING SCHEDULE	
4 PERFORMING ORGANIZATION REPORT NUMBER(S) NPS-PH-92-002	5 MONITORING ORGANIZATION REPORT NUMBER(S)
6a NAME OF PERFORMING ORGANIZATION Naval Postgraduate School 6b OFFICE SYMBOL (If applicable) PH	7a NAME OF MONITORING ORGANIZATION Naval Postgraduate School
6c ADDRESS (City, State, and ZIP Code) Monterey, CA 93943-5000	7b ADDRESS (City, State, and ZIP Code) Monterey, CA 93943-5000
8a NAME OF FUNDING/SPONSORING ORGANIZATION Naval Postgraduate School 8b OFFICE SYMBOL (If applicable)	9 PROCUREMENT INSTRUMENT IDENTIFICATION NUMBER OM&N Direct Funding
8c ADDRESS (City, State, and ZIP Code) Monterey, CA 93943-5000	10 SOURCE OF FUNDING NUMBERS PROGRAM ELEMENT NO / PROJECT NO / TASK NO / WORK UNIT ACCESSION NO

11 TITLE (Include Security Classification)
ON THE USE OF SYMPATHETIC RESONATORS TO IMPROVE LOW-FREQUENCY UNDERWATER TRANSDUCER PERFORMANCE (UNCLASSIFIED)

12 PERSONAL AUTHOR(S)
S. R. BAKER AND J. M. ELLSWORTH

13a TYPE OF REPORT	13b TIME COVERED	14 DATE OF REPORT (Year, Month, Day)	15 PAGE COUNT
Technical Report	FROM Jan 90 TO Sep 90	1991 October	72

16 SUPPLEMENTARY NOTATION

17 COSATI CODES			18 SUBJECT TERMS (Continue on reverse if necessary and identify by block number)
FIELD	GROUP	SUB-GROUP	Low Frequency Active, Multiple-scattering, Sympathetic Resonator, Quasiresonance, Coupled-Network, Array

19 ABSTRACT (Continue on reverse if necessary and identify by block number)

The achievable gain in the radiation resistance and directivity of a low-frequency underwater transducer due to the presence of an array of sympathetic resonators has been analyzed. The resonators were all taken to be air bubbles, and both the resonators and transducer were taken to be compact ($ka << 1$). The resonators were taken to be equally spaced around a circle of radius R, with the transducer located on the axis. The gain was calculated for various numbers of resonators as a function of $ka_{resonator}$, $ka_{transducer}$ and kR, for the transducer in the plane of the resonators and out of the plane a distance of one-quarter wavelength. For the transducer in the plane, a gain in radiation resistance of approximately two is possible with six or more resonators. For the transducer out of the plane, it is shown that a front-to-back discrimination of approximately 8 dB can be achieved, at the expense of a decrease of approximately ten percent in the achievable gain in the radiation resistance, compared to the transducer in the plane of the resonators.

20 DISTRIBUTION/AVAILABILITY OF ABSTRACT	21 ABSTRACT SECURITY CLASSIFICATION
☒ UNCLASSIFIED/UNLIMITED ☐ SAME AS RPT ☐ DTIC USERS	UNCLASSIFIED
22a NAME OF RESPONSIBLE INDIVIDUAL Steven R. Baker	22b TELEPHONE (Include Area Code) 408-646-2732 / 22c OFFICE SYMBOL PH/Ba

ABSTRACT

The achievable gain in the radiation resistance and directivity of a low-frequency underwater transducer due to the presence of an array of sympathetic resonators has been analyzed. The resonators were all taken to be air bubbles, and both the resonators and transducer were taken to be compact ($ka << 1$). The resonators were taken to be equally spaced around a circle of radius R, with the transducer located on the axis. The gain was calculated for various numbers of resonators as a function of $ka_{resonator}$, $ka_{transducer}$ and kR, for the transducer in the plane of the resonators and out of the plane a distance of one-quarter wavelength. For the transducer in the plane, a gain in radiation resistance of approximately two is possible with six or more resonators. For the transducer out of the plane, it is shown that a front-to-back discrimination of approximately 8 dB can be achieved, at the expense of a decrease of approximately ten percent in the achievable gain in the radiation resistance, compared to the transducer in the plane of the resonators.

ACKNOWLEDGEMENTS

Much of this report is based upon the Masters degree thesis of LT John M. Ellsworth.

The work reported herein was supported by the Naval Postgraduate School.

TABLE OF CONTENTS

LIST OF FIGURES

LIST OF TABLES

I. INTRODUCTION

A. BACKGROUND

I. Tolstoy [Ref. 1, Ref. 2], and A. Tolstoy and I. Tolstoy [Ref. 3] have recently analyzed the multiple-scattering of sound from a collection of compact ($ka << 1$) monopole scatterers (e.g. gas-filled bubbles, gas-filled balloons, and thin shells) in water, insonified by a simple harmonic plane-wave at frequencies close to the resonance frequency of an individual scatterer. The response of these systems was quantified by computing the ratio of the scattered pressure on the surface of a scatterer in the presence of the other scatterers to that of the incident plane wave. This ratio was defined as the amplification factor, μ. They investigated the value of this amplification factor for various simple geometrical arrangements of monopole resonant scatterers, and showed that amplification factors of the order of 10^2 were to be expected for air bubbles in water at one atmosphere ambient pressure (The amplification factor of a single bubble is about 70.). These systems were said to be "quasiresonant".

I. Tolstoy [Ref. 4] has also recently analyzed the strength and directionality of the resonant multiple-scattering of sound from a linear array of compact monopole resonant scatterers insonified by a simple harmonic plane wave. He reports that "quasiresonance" effects exhibit strong directionality in this system, with amplification factors of up to 700. The potential application of resonant multiple-scattering, or "quasiresonance", in Tolstoy's words, to improve the performance of a low frequency active sonar transducer is the subject

of the research described in this report.

B. OBJECTIVES

The objectives of this research are multiple. The first is to reproduce I. Tolstoy's results using network analysis, a tool familiar to the transducer and array designer. It will be shown that network analysis gives results identical to Tolstoy's analysis. The existence of quasiresonance will then applied to a circular array of scatterers, where the incident plane wave is replaced by an active transducer located on the axis of the circle and radiating spherical waves. The acoustic advantage gained in this system will be quantified by the gain in the radiation resistance seen by the transducer by the introduction of the array of scatterers. An increase in radiation resistance enables the transfer of more power to the acoustic field for a given surface velocity of the transducer (High power low frequency active sonar transducers tend to be resonant devices that are displacement limited.). The cases of the transducer in the plane of the circle and displaced by one-quarter wavelength out of the plane will be analyzed for both their increase in radiation resistance and gain in directivity over that of a single transducer.

II. THEORY

A. INTRODUCTION

For simple configurations of compact resonant scatterers insonified by a simple harmonic plane wave, Tolstoy predicted the existence of so-called "quasiresonance" using multiple-scattering theory (Quasiresonance is Tolstoy's term for the dramatic enhancement of the scattered field of a resonant scatterer as a result of resonant multiple-scattering.). Tolstoy's analysis will be reviewed and applied to the simplest case of the scattering of a plane-wave axially incident upon a pair of resonant scatterers in Section B. In Section C the same problem is treated using network analysis. It will be shown that this method produces results identical to Tolstoy's.

B. TOLSTOY'S ANALYSIS OF RESONANT MULTIPLE-SCATTERING

Tolstoy's analysis of the multiple-scattering of a plane wave incident upon a collection of compact resonant scatterers proceeds using the linear theory of acoustics. The following development parallels that of Reference [1] and Reference [3], with the difference being that here all time-harmonic functions are taken to be of the form $e^{j\omega t}$. This will result in minor differences in the appearance of otherwise equivalent equations.

Consider first the case of a single resonant scatterer insonified by an incident plane-wave. The scatterer is taken to be an air-filled bubble of radius a, which is assumed small compared to the acoustic wavelength ($ka << 1$). From Kinsler, Frey, Coppens, and Sanders [Ref.

5, p. 230], the ratio of the scattered pressure on the surface of the bubble to the free-field pressure of an incident plane-wave is, in the notation adopted here (note: the minus sign in Eq. 2-1, which is not present in Eq. 10-22 of Ref. 5, results from the assumed convention of positive velocity directed into the water):

$$\frac{p^{sc}_{single}(a)}{p^f} = -\frac{R_r + j\omega m_r}{(R_m + R_r) + j(\omega m_r - s/\omega)}, \qquad (2\text{-}1)$$

where:

$p^{sc}_{single}(a)$ = scattered acoustic pressure on the bubble surface,
p^f = incident free field acoustic pressure,
R_r = bubble mechanical radiation resistance,
m_r = bubble mechanical radiation mass,
R_m = bubble internal mechanical resistance,
s = bubble internal mechanical stiffness.

The scattered pressure at any distance r, $p^{sc}_{single}(r)$, is related to the scattered pressure at the surface by

$$\frac{p^{sc}_{single}(r)}{p^{sc}_{single}(a)} = \frac{a}{r}\frac{e^{-jkr}}{e^{-jkr}} \cong \frac{e^{-jkr}}{jkr}\frac{jka}{(1 - jka)}, \qquad (2\text{-}2)$$

where the approximation ka << 1 has been used. Combining Eq. 2-1 and Eq. 2-2 results in the following expression for the ratio of the scattered acoustic pressure at some radius r from the scatterer, $p^{sc}_{single}(r)$, to that of the incident pressure, p^f:

$$\frac{p^{sc}_{single}(r)}{p^f} = \frac{1}{jkr}\left(\frac{1}{1 - j\zeta}\right)e^{-jkr}, \qquad (2\text{-}3)$$

where:

$$\zeta = \frac{(\omega_0^2/\omega^2 - 1)}{ka}$$

and

$$\frac{\omega_0}{\omega} = \sqrt{\frac{3\gamma P_0}{\rho c^2 (ka)^2}} \ . \qquad (2\text{-}4)$$

In deriving Eq. 2-3, the following assumptions and substitutions have been made:

(1) Surface tension is neglected, so the only mechanical stiffness of the bubble is due to internal gas (air) pressure;
(2) The bubble internal mechanical losses due to viscosity and thermal conductivity are neglected compared to the acoustic radiation loss, i.e. $R_m << R_r$;
(3) $R_r = \omega_0 m_r / Q$;
(4) $Q = 1/(ka)$;
(5) $s = \omega_0^2 m_r$;
(6) $ka << 1$;
(7) $\omega \approx \omega_0$.

It follows from Eq. 2-3 that the ratio of the scattered acoustic pressure on the single scatterer's surface to that of the incident free-field pressure can be written:

$$\frac{p^{sc}_{single}}{p^f} = \frac{1}{jka}\left(\frac{1}{1 - j\zeta}\right) e^{-jka} \ . \qquad (2\text{-}5)$$

Tolstoy introduces the quantities F_a and A by rewriting Equation 2-3 as Equation 2-6.

$$F_a = \frac{p^{sc}_{single}(r)}{p^f} = A\,\frac{e^{-jkr}}{jkr} \ , \qquad (2\text{-}6)$$

where:

$$A = \frac{1}{1 - j\zeta} \ .$$

F_a is the normalized scattered acoustic pressure for a single scatterer insonified by an incident plane-wave and A is the single-scattering amplitude coefficient.

Now consider a system of N identical interacting scatterers insonified by a plane-wave. Let $p_n^{sc}(r)$ represent the scattered acoustic pressure. An equation for $p_n^{sc}(r)/p^f$, equivalent to that of Equation 2-6 for a single scatterer, can be written as Equation 2-7 for the multiple-scattering case:

$$F_{b_n} = \frac{p_n^{sc}(r)}{p_n^f} = B_n \frac{e^{-jkr}}{jkr} . \qquad (2\text{-}7)$$

F_{b_n} is the normalized scattered acoustic pressure from scatterer n, insonified by both the incident plane-wave and the fields of the other scatterers, p_n^f is the free-field pressure of the incident plane-wave at scatterer n, and B_n is the multiple scattering amplitude coefficient for scatterer n.

The response of a scatterer to multiple incident pressure fields can be evaluated by summing up the response to each individual incident pressure field [Ref. 3]. For a system of N scatterers, this results in Equation 2-8 for the scattered field at the surface of the n^{th} resonator:

$$B_n \frac{e^{-jka_n}}{jka_n} = A_n \left(1 + \sum_{m \neq n} B_m \frac{e^{-jkl_{nm}}}{jkl_{nm}} e^{j\psi_{nm}} \right) \frac{e^{-jka_n}}{jka_n} , \qquad (2\text{-}8)$$

where: ψ_{nm} is the phase difference in the incident plane wave between resonator m and n, and m = 1...N. The subscript notation for A has been added to allow for a system of different-sized scatterers.

Tolstoy defines the amplification factor μ (different from the scattering amplitude coefficient mentioned previously) to be the magnitude of the ratio of the scattered acoustic pressure on the surface of a scatterer, p_n^{sc}, to the free-field acoustic pressure of the incident plane-wave, p_n^f. With this definition, Equation 2-9 follows from Equation 2-7:

$$\mu_n = \left|\frac{p_n^{sc}}{p_h^f}\right| = \frac{|B_n|}{ka_n} . \qquad (2\text{-}9)$$

Tolstoy denotes the amplification factor for a single scatterer as μ_0. Equation 2-10, then, follows from Equation 2-6.

$$\mu_{0_n} = \left|\frac{p^{sc}_{single_n}}{p_h^f}\right| = \frac{|A_n|}{ka_n} . \qquad (2\text{-}10)$$

From Equations 2-9 and 2-10, the gain in the amplification factor due to multiple-scattering, μ/μ_0, is expressed in terms of B_n/A_n by Equation 2-11:

$$\frac{\mu_n}{\mu_{0_n}} = \left|\frac{p_n^{sc}}{p^{sc}_{single_n}}\right| = |B_n/A_n| . \qquad (2\text{-}11)$$

B.1. APPLICATION OF TOLSTOY'S METHOD TO A SYSTEM OF TWO RESONANT-SCATTERERS

As an example application, Tolstoy considered a system of two identical resonators insonified by a plane-wave traveling along the axis joining their centers, as shown in Figure 2-1.

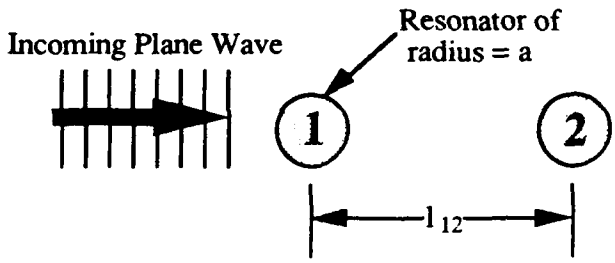

Figure 2-1. A two-resonator system insonified by a plane-wave along the axis of the resonators.

Application of Equation 2-8 to the situation shown in Figure 2-1

results in the set of Equations 2-12:

$$B_1 \frac{e^{-jka}}{jka} = A \frac{e^{-jka}}{jka} + A \frac{e^{-jka}}{jka} B_2 \frac{e^{-jkl}}{jkl} e^{-jkl}, \qquad (2\text{-}12)$$

$$B_2 \frac{e^{-jka}}{jka} = A \frac{e^{-jka}}{jka} + A \frac{e^{-jka}}{jka} B_1 \frac{e^{-jkl}}{jkl} e^{-jkl}.$$

For a system of identical scatterers, the values of A_1 and A_2 are equal; therefore, the subscript on A in Equation 2-12 has been omitted. Since all variables in Equation 2-12 are known except B_1 and B_2, one can solve for B_1/A in terms of A and kl, resulting in Equation 2-13:

$$B_1/A = \frac{1 + \left(A \frac{e^{-jkl}}{jkl}\right) e^{-jkl}}{1 - \left(A \frac{e^{-jkl}}{jkl}\right)^2}. \qquad (2\text{-}13)$$

Substituting the expressions for ζ and ω/ω_0 for an air-filled bubble into the expression for A, B_1/A is given in terms of the variables ka, kl, c, P_0, and ρ by Equation 2-14:

$$B_1/A = \frac{p_1^{sc}}{p_{single}^{sc}} = \frac{1 - e^{-jkl}\left(\dfrac{\frac{ka}{kl} e^{j(ka - kl)}}{\rho c\left((ka)^2 + j\left(ka - \frac{3\gamma P_0}{\rho c^2 (ka)}\right)\right)}\right)}{1 - \left(\dfrac{\frac{ka}{kl} e^{j(ka - kl)}}{\rho c\left((ka)^2 + j\left(ka - \frac{3\gamma P_0}{\rho c^2 (ka)}\right)\right)}\right)^2}. \qquad (2\text{-}14)$$

For bubbles just under the surface of the ocean:

P_0 = 10132 Pa (1 atmosphere)
ρ = 998 kg m^{-3}
c = 1498 m s^{-1}

As observed by Tolstoy [Ref. 3], plots of Equation 2-14 display spurious peaks. Following Tolstoy, then, the data used to produce the

graphs of $|B_1/A|$ versus ka and kl, plotted in Figures 2-2a,b, have been treated to limit peaks in bounded intervals of width less than 2ka (According to Tolstoy, peaks narrower than 2ka, where 2a equals the resonator diameter, are not meaningful, since the pressure over a compact resonator is approximately constant.). The process used involved comparing three consecutive values of $|B_1/A|$ in the kl direction for each value of ka (Three consecutive points in the kl direction span approximately 2ka.). If the value of $|B_1/A|$ for the middle point was greater than either of its neighboring points (a peak) then this value was set equal to the mean of the two neighboring points. This procedure was repeated several times to obtain the desired smoothing.

Figures 2-2a,b show a maximum response of $|B_1/A|$ equal to 5.5 at approximately ka = 0.01393 and kl = 0.60. As a result of multiple-scattering, then, the scattered pressure amplitude of the first bubble is 5.5 times greater in the presence of the second bubble than in its absence. Additionally, the value of ka at the maximum response is shifted from that for a single resonant bubble of 0.01379.

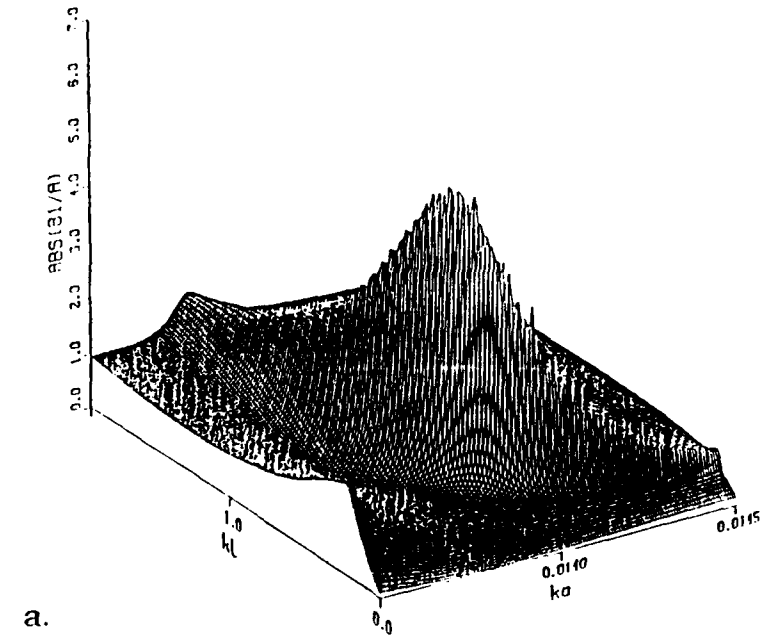

a.

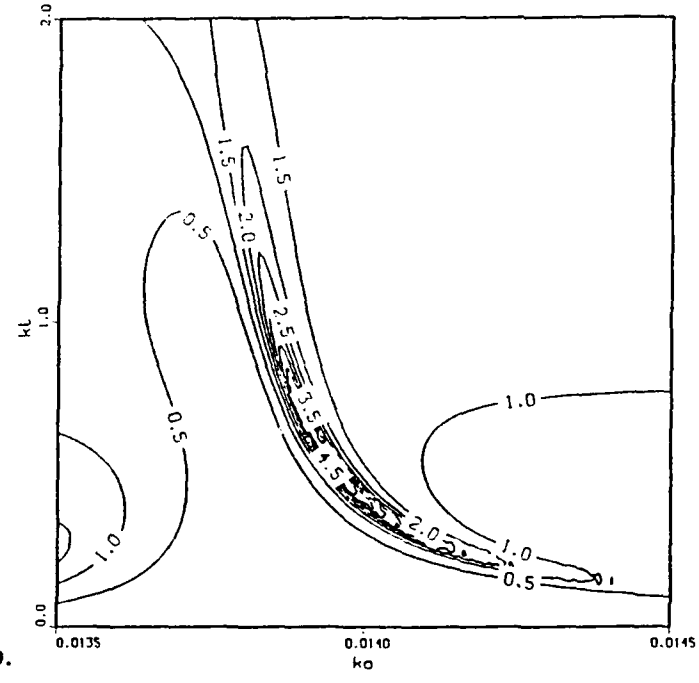

b.

Figure 2-2a,b. Surface (a), and contour (b) plots showing $|B_1/A|$ for the double-resonator system as a function of ka and kl for axial incidence of the plane-wave.

C. NETWORK ANALYSIS OF RESONANT MULTIPLE-SCATTERING

Figure 2-3 displays a network model of N interacting scatterers insonified by an incident acoustic wave (Note: pressure (p) and volume velocity (U_n) are chosen as the mechanical variables, and the direction of positive velocity is clockwise.).

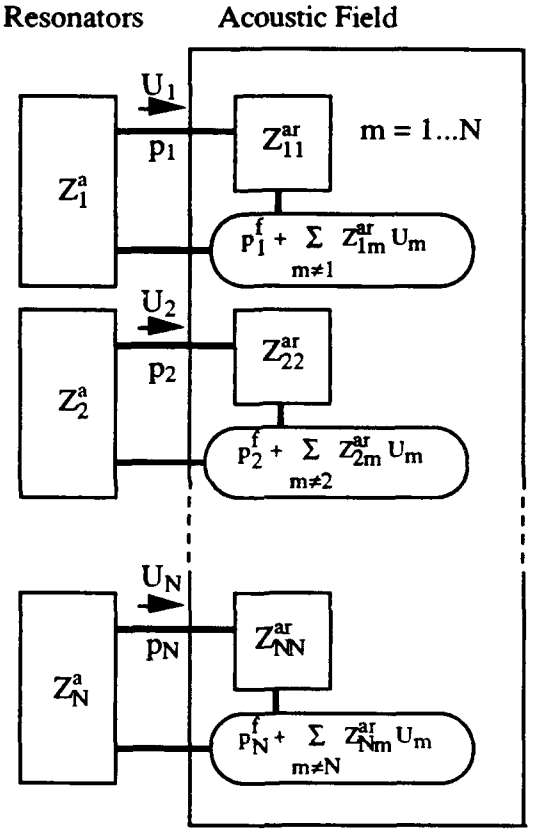

Figure 2-3. Network model of N interacting resonators insonified by a plane-wave.

The network equations for Figure 2-3 are:

$$p_n = p_h^f + \sum_{m=1}^{N} Z_{nm}^{ar} U_m \qquad p_n = - Z_n^a U_n \,, \tag{2-15}$$

where:

p_n = Surface pressure at element n,

p_n^f = Free field pressure at element n due to an externally incident field only,
U_n = Volume velocity of element n,
Z_{an} = Acoustic impedance of element n,
Z_{nn}^{ar} = Acoustic radiation impedance seen by element n with all other elements blocked ($U_{m \neq n} = 0$; m=1...N),
Z_{nm}^{ar} = Acoustic transfer impedance from element m to element n.

Neglecting the effects of surface tension, thermal relaxation, etc., the intrinsic acoustic impedance of a small (ka << 1) gas-filled bubble can be approximated by one of reactance only, given by Kinsler, Frey, Coppens and Sanders [Ref. 5] as Equation 2-16:

$$Z_n^a = j \frac{-3\gamma P_0}{c(ka_n)} S_n^{-1} , \qquad (2-16)$$

where:

a_n = radius of element n;
c = speed of sound in water;
k = wave number, ω/c;
P_0 = ambient pressure of environment;
S_n = surface area of element n;
γ = ratio of specific heats (air).

The self acoustic radiation impedance seen by element n, Z_{nn}^{ar}, can be approximated by Equation 2-17.

$$Z_{nn}^{ar} = \rho c \left((ka_n)^2 + jka_n\right) S_n^{-1} , \qquad (2-17)$$

where ρ is the density of water. Equation 2-17 is the acoustic radiation impedance presented to a compact source with no other active or scattering elements present. It is also the acoustic radiation impedance seen by a compact source in the presence of other compact sources when these sources are blocked ($U_{m \neq n} = 0$; m =

1...N).

The acoustic transfer impedance from element m to element n is given by Equation 2-18:

$$Z^{ar}_{nm} = Z^{ar}_{mm}\frac{ka_m}{kl_{nm}}e^{j(ka_m - kl_{nm})} . \qquad (2\text{-}18)$$

In matrix form, the network equations (Equation 2-15) can be written as Equation 2-19:

$$\{p_n\} = [Z^{ar}_{nm}]\{U_m\} + \{p^f_n\} ; \quad m,n = 1...N , \qquad (2\text{-}19)$$

where:

$\{X_n\}$;	n = 1...N	A 1xN column matrix, N elements.
$[X_{nm}]$;	n,m = 1...N	A NxN square matrix, N^2 elements.

Substituting $p_n = -Z^a_n U_n$ and rearranging results in Equation 2-20:

$$\{-p^f_n\} = [Z^{ar}_{nm} + Z^a_n\delta_{nm}]\{U_m\} ; \quad m,n = 1...N , \qquad (2\text{-}20)$$

where δ_{nm} is the Kronecker delta function:

$$\delta_{nm} = \begin{cases} 1; & m = n \\ 0; & m \neq n \end{cases} .$$

C.1. APPLICATION OF NETWORK ANALYSIS TO A SYSTEM OF TWO RESONANT-SCATTERERS

Modeling the system of two scatterers shown in Figure 2-1 as a network, Equation 2-20 becomes Equation 2-21:

$$\begin{vmatrix} -p^f_1 \\ -p^f_2 \end{vmatrix} = \begin{vmatrix} Z^{ar}_{11} + Z^a_1 & Z^{ar}_{12} \\ Z^{ar}_{21} & Z^{ar}_{22} + Z^a_2 \end{vmatrix} \begin{vmatrix} U_1 \\ U_2 \end{vmatrix} . \qquad (2\text{-}21)$$

Using the relation $p^{sc}_n = Z^{ar}_{nn}U_n$ to eliminate U_n, the above equations

can be written in terms of the scattered acoustic pressure at each individual resonator, p_n^{sc}, and the incident plane-wave pressures, as given by Equation set 2-22:

$$p_1^{sc} = (p_1^f + C_{12}\, p_2^{sc})\, D_1^{-1} , \qquad (2\text{-}22)$$

$$p_2^{sc} = (p_2^f + C_{21}\, p_1^{sc})\, D_2^{-1} ,$$

where

$$C_{nm} = \frac{Z_{nm}^{ar}}{Z_{mm}^{ar}}$$

and

$$D_n = -\frac{Z_{nn}^{ar} + Z_n^a}{Z_{nn}^{ar}} .$$

For a system of identical resonators, C_{nm} and D_n are the same for all m and n; therefore the subscript notation is not required. Solving Equation 2-22 for the scattered acoustic pressure at each resonator in terms of the incident plane-wave pressure results in Equation 2-23 for the scattered pressure at resonator one:

$$p_1^{sc} = \frac{p_1^f D + p_2^f C}{D^2 - C^2} . \qquad (2\text{-}23)$$

The scattered acoustic pressure at the first resonator in the absence of the second resonator, $p_{single_1}^{sc}$, is obtained using Equation 2-23 by letting the transfer coefficient C equal zero, resulting in Equation 2-24:

$$p_{single_1}^{sc} = \frac{p_1^f}{D} . \qquad (2\text{-}24)$$

Dividing equation Equation 2-23 by Equation 2-24 results in Equation 2-25 for the ratio B_1/A as defined by Tolstoy:

$$B_1/A = \frac{p_1^{sc}}{p_{single_1}^{sc}} = \frac{1 + (p_2^f/p_1^f)\left(\frac{C}{D}\right)}{1 - \left(\frac{C}{D}\right)^2} \quad . \tag{2-25}$$

Inserting Equations 2-16 thru 2-18 into Equation 2-25, one obtains an equation for B_1/A in terms of the variables ka, kl, c, P_0, p_1^f, p_2^f, and ρ, as given by Equation 2-26:

$$B_1/A = \frac{p_1^{sc}}{p_{single_1}^{sc}} = \frac{1 - (p_2^f/p_1^f)\left(\frac{\frac{ka}{kl} e^{j(ka - kl)}}{\rho c\left((ka)^2 + j\left(ka - \frac{3\gamma P_0}{\rho c^2 (ka)}\right)\right)}\right)}{1 - \left(\frac{\frac{ka}{kl} e^{j(ka - kl)}}{\rho c\left((ka)^2 + j\left(ka - \frac{3\gamma P_0}{\rho c^2 (ka)}\right)\right)}\right)^2} \quad . \tag{2-26}$$

The incident plane wave pressures p_1^f and p_2^f are of equal magnitude and differ only by the phase factor $e^{jkl_{12}}$, resulting in Equation 2-27:

$$\frac{p_2^f}{p_1^f} = e^{-jkl} \quad . \tag{2-27}$$

Substituting this expression into Equation 2-26, one obtains Equation 2-28:

$$B_1/A = \frac{p_1^{sc}}{p_{single_1}^{sc}} = \frac{1 - e^{-jkl}\left(\frac{\frac{ka}{kl} e^{j(ka - kl)}}{\rho c\left((ka)^2 + j\left(ka - \frac{3\gamma P_0}{\rho c^2 (ka)}\right)\right)}\right)}{1 - \left(\frac{\frac{ka}{kl} e^{j(ka - kl)}}{\rho c\left((ka)^2 + j\left(ka - \frac{3\gamma P_0}{\rho c^2 (ka)}\right)\right)}\right)^2} \quad . \tag{2-28}$$

Equation 2-28 is identical to Equation 2-14, demonstrating the equivalence of Tolstoy's method and network analysis.

D. NETWORK ANALYSIS OF A TRANSDUCER INTERACTING WITH MULTIPLE RESONANT-SCATTERERS

Network analysis will now be applied to the problem of a compact transducer in the presence of an array of interacting, compact resonant scatterers. The procedure is the same here as in section C, except that the incident plane wave is replaced by an outward-traveling spherical wave whose source is a compact transducer. A network model of the transducer and N resonator system is shown in Figure 2-4.

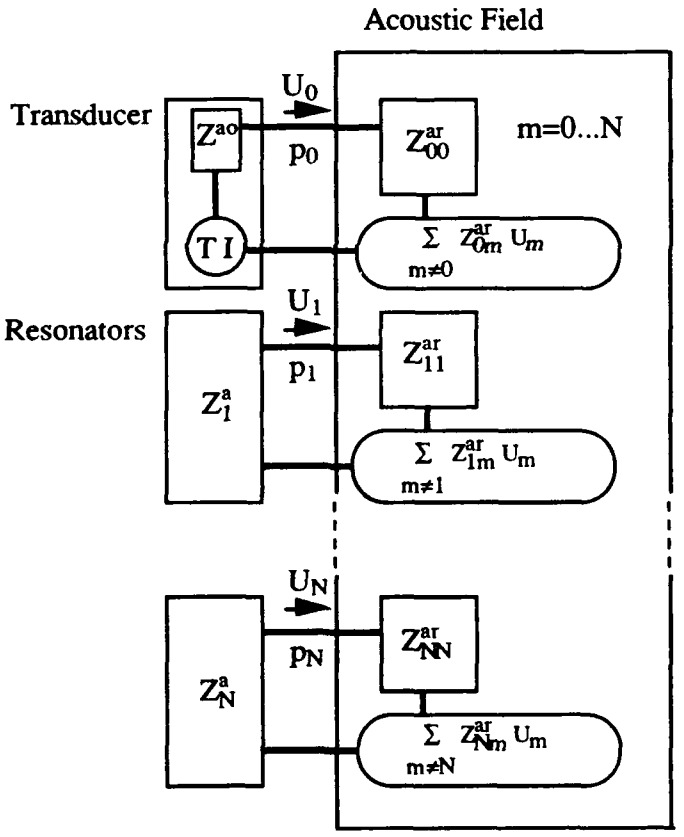

Figure 2-4. Network model of a single transducer and N interacting resonators.

The network equations for Figure 2-4 are:

$$p_0 = TI - Z^{ao}\, U_0\,, \qquad p_n = -\, Z^a_n\, U_n\;;\; n = 1..N, \tag{2-29a}$$

$$p_n = \sum_m Z^{ar}_{nm} U_m\;;\; m,n = 0..N, \tag{2-29b}$$

where

T = transduction coefficient;
Z^{ao} = transducer open circuit (I = 0) acoustic impedance,

and the subscript n = 0 denotes the transducer, $n \neq 0$ a resonator.

The transducer open-circuit acoustic impedance (Z^{ao}) and transduction coefficient (T) are shown only for completeness and will not be considered further, as the quantity of interest will be the radiation impedance presented to the transducer.

Using the network Equations 2-29, the matrix equation for the network model shown in Figure 2-4 is given by Equation 2-30:

$$\begin{vmatrix} p_0 \\ \{p_n\} \end{vmatrix} = \begin{vmatrix} Z^{ar}_{00} & \{Z^{ar}_{m0}\}^T \\ \{Z^{ar}_{n0}\} & [Z^{ar}_{nm}] \end{vmatrix} \begin{vmatrix} U_0 \\ \{U_m\} \end{vmatrix};\; n, m = 1...N, \tag{2-30}$$

where

$\{X_n\}$, n = 1...N denotes a 1xN column matrix, N elements,
$[X_{nm}]$, n,m = 1...N denotes a NxN square matrix, N^2 elements,

and the superscript T denotes transpose. Replacing the 1 x N surface pressure matrix, $\{p_n\}$, with $\{-\, Z^a_n U_n\}$, and then normalizing by U_0, the transducer volume velocity, Equation 2-30 becomes Equation 2-31:

$$\begin{vmatrix} Z^{ar}_{total} \\ \{0\} \end{vmatrix} = \begin{vmatrix} Z^{ar}_{00} & \{Z^{ar}_{m0}\}^T \\ \{Z^{ar}_{n0}\} & [Z^{ar}_{nm} + Z^a_n \delta_{nm}] \end{vmatrix} \begin{vmatrix} 1 \\ \{U^{rel}_m\} \end{vmatrix};\; n,m = 1...N, \tag{2-31}$$

where

Z^{ar}_{total} = total acoustic radiation impedance seen by the transducer;

U_m^{rel} = ratio of element m's volume velocity to that of the transducer ($U_m^{rel} = U_m/U_0$).

Equation 2-31 can be written as two separate matrix equations, Equations 2-32a,b:

$$Z_{total}^{ar} = Z_{00}^{ar} + \{Z_{m0}^{ar}\}^T \{U_m^{rel}\}, \qquad (2\text{-}32a)$$

$$\{0\} = \{Z_{n0}^{ar}\} + [Z_{nm}^{ar} + Z_n^a \delta_{nm}] \{U_m^{rel}\}. \qquad (2\text{-}32b)$$

Solving Equation 2-32b for $\{U_m^{rel}\}$ by matrix inversion and substituting the result into Equation 2-32a, one obtains Equation 2-33, the total acoustic radiation impedance seen by the transducer.

$$Z_{total}^{ar} = Z_{00}^{ar} - \{Z_{m0}^{ar}\}^T [Z_{nm}^{ar} + Z_n^a \delta_{nm}]^{-1} \{Z_{n0}^{ar}\}. \qquad (2\text{-}33)$$

Equation 2-33 expresses this impedance in terms of the radiation and transfer impedances of the individual elements.

The total acoustic power radiated by the transducer is given by Equation 2-34.

$$\Pi = \frac{1}{2} |U_0|^2 \, Re(Z_{total}^{ar}). \qquad (2\text{-}34)$$

The gain in power delivered to the acoustic field due to the addition of the sympathetic resonators equals the ratio of total power delivered with the resonators present to the power delivered when they are absent, $\Pi_0 = \frac{1}{2} |U_0|^2 \, Re(Z_{00}^{ar})$. For a displacement-limited source, typical of a sonar projector operated near its resonant frequency, this ratio reduces to the ratio of the radiation resistances for the two cases. This gain factor is expressed as Equation 2-35:

$$G_R = \frac{Re(Z_{total}^{ar})}{Re(Z_{00}^{ar})}. \qquad (2\text{-}35)$$

III. ANALYSIS

A. INTRODUCTION

The theory developed in the previous chapter will now be applied to two specific geometric configurations of a transducer and N identical resonators: a "planar" and a "conical" configuration. The resonators will be treated as simple gas-filled bubbles. It is assumed throughout that the acoustic wavelength is much larger than the dimensions of either the transducer or the resonators. For initial calculations, ambient pressure is taken to be one atmosphere, and the radius of the transducer is taken to be equal to that of the resonators ($ka_0 = ka_n$). Later, calculations will be presented for the case of an ambient pressure of 50 atmospheres, and the restriction $ka_0 = ka_n$ will be relaxed.

B. ANALYSIS OF PLANAR CONFIGURATION

The geometry of the first arrangement to be analyzed is shown in Figure 3-1. It consists of N identical resonators, equally spaced around a circle of radius l_{n0}. This geometric arrangement will be referred to as the planar configuration.

For the configuration shown in Figure 3-1, Equation 2-35 becomes Equation 3-1:

$$G_R = \frac{\mathrm{Re}\left(Z_{00}^{ar} - \{Z_{mo}^{ar}\}^T \left[Z_{nm}^{ar} + Z_n^a \delta_{nm}\right]^{-1} \{Z_{no}^{ar}\} \right)}{\mathrm{Re}\left(Z_{00}^{ar} \right)} \; ; \quad n,m = 1...4 \qquad (3\text{-}1)$$

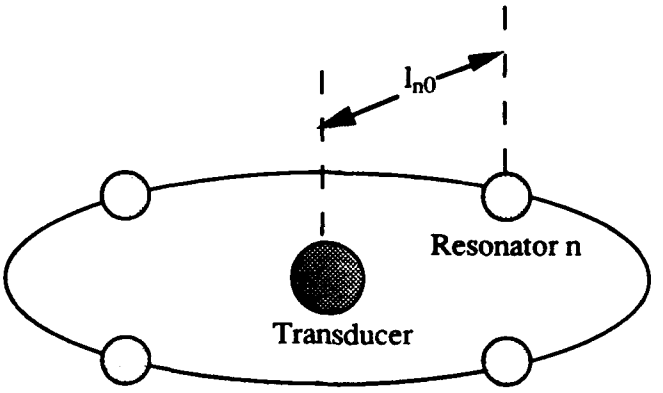

Figure 3-1. Resonators equally spaced around transducer in a planar configuration of radius l_{n0}, N=4.

Using Equations 2-16, 17, and 18, and canceling the common surface areas S_n, Equation 3-1 can be written in terms of specific acoustic impedances as Equation 3-2:

$$G_R = \frac{\mathrm{Re}\left(z_{00}^{ar} - \{z_{n0}^{ar}\}^T \left[z_{nm}^{ar} + z_n^a \delta_{nm}\right]^{-1} \{z_{n0}^{ar}\}\right)}{\mathrm{Re}(z_{00}^{ar})} \; ; \quad n,m = 1...4 \qquad (3\text{-}2)$$

where:

$$z_{00}^{ar} = \rho c \left((ka)^2 + jka\right),$$

$$z_{nm}^{ar} + z_n^a \delta_{nm} = \rho c \left((ka)^2 + jka\right) - j \frac{3\gamma P_0}{c(ka)} \; ; \quad n = m,$$

$$z_{nm}^{ar} + z_n^a \delta_{nm} = z_{nm}^{ar} = \rho c \left((ka)^2 + jka\right) \frac{ka}{kl_{nm}} \, e^{j(ka - kl_{nm})} \; ; \quad n \neq m,$$

$$z_{n0}^{ar} = \rho c \left((ka)^2 + jka\right) \frac{ka}{kl_{n0}} \, e^{j(ka - kl_{n0})} \quad ,$$

and l_{nm} is the distance between element n and m, the subscript 0 denoting the transducer. Using simple trigonometry, kl_{nm} for $n,m \neq 0$ can be written in terms of m, n, and kl_{n0} for the planar case as Equation 3-3:

$$kl_{nm} = kl_{n0}\, 2 \sin\left(\frac{\pi}{N}|n - m|\right); \quad n,m = 1...N. \qquad (3\text{-}3)$$

Using Equations 3-2 and 3-3, the gain in radiation resistance seen by the transducer, G_R, can be expressed in terms of ka and kl_{n0}.

The gain in radiation resistance for the N = 4 planar configuration can be plotted in the form of surface and contour plots using Equation 3-1, as shown in Figures 3-2a and 2b. It should be pointed out that here and in all subsequent surface plots of G_R, no spurious peaks were observed, and no smoothing has been applied. Inspection of these graphs reveals two local maxima, one of magnitude 4.34 at ka = 0.975 ka_r, kl_{n0} = 0.5, and another of magnitude 1.79 at ka = 1.005 ka_r, kl_{n0} = 2.7, where ka_r equals 0.01379, the resonance value of ka for a single air-filled bubble at one atmosphere ambient pressure. The local maximum at ka = 0.975 ka_r, kl_{n0} = 0.5 is an artifact of the range of kl_{n0} chosen. In fact, the gain in radiation resistance diverges as $(kl_{n0})^{-1}$ as kl_{n0} approaches zero. This case is uninteresting and will not be considered further. The interesting local maximum at ka = 1.005 ka_r, kl_{n0} = 2.7 represents a gain of almost a factor of two in the radiation resistance seen by the transducer. Note that kl = π corresponds to a separation distance of one-half wavelength. For the N = 4 planar configuration, then, the maximum gain in radiation resistance is obtained when the resonators are located a distance just under one-half wavelength from the transducer.

The gain in radiation resistance for the planar configuration where N is set equal to eight and fifteen is shown in Figures 3-2c thru 3-2f. These plots display similar characteristics to the N = 4 case. All show a local maximum of magnitude approximately two at ka $\cong$ ka_r = 0.01379 and $kl_{n0} \cong \pi$.

The local maximum values for G_R at $kl_{n0} \cong \pi$, $ka \cong ka_r = 0.01379$ for various values of N ranging from 2 to 25 and their associated parameters are tabulated in Table 3-1. Two major points can be observed from Table 3-1. First, the resonant bubbles' volume velocity leads the transducer's by a phase shift of 90° (equivalent to - 270°). This phase shift is created in two parts. Since the separation between transducer and resonator is approximately one-half wavelength, this introduces a shift of - 180° in phase due to simple wave propagation. The remaining - 90° is introduced at the surface of a compact resonating bubble between the incident and scattered wave, as predicted by Equation 2-24. Second, note that little is gained as one increases the number of resonators beyond about four.

N	G_R	ka_{max}	kl_{max}	$mag(U_n^{rel})$	$arg(U_n^{rel})$
2	1.26	0.01382	2.65	0.395	90.0°
4	1.87	0.01383	2.82	0.649	90.0°
6	1.96	0.01385	2.87	0.474	90.0°
8	1.96	0.01386	2.87	0.356	90.0°
10	1.96	0.01386	2.87	0.285	90.0°
15	1.96	0.01385	2.87	0.190	90.0°
20	1.96	0.01381	2.87	0.142	90.0°
25	1.96	0.01376	2.87	0.114	90.0°

Table 3-1. Values of G_R for N ranging from 2 to 25 and the parameters associated with the local maximum at $kl_{n0} \cong \pi$, $ka \cong ka_r = 0.01379$. Planar configuration.

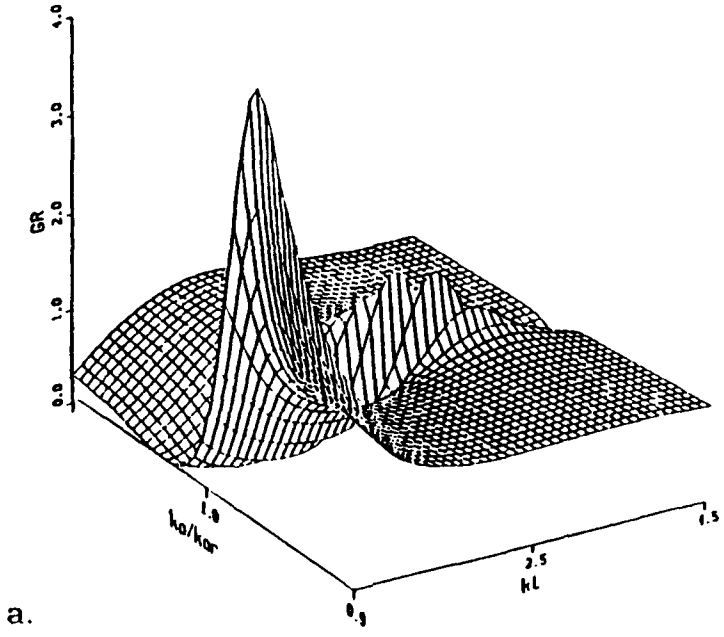

a.

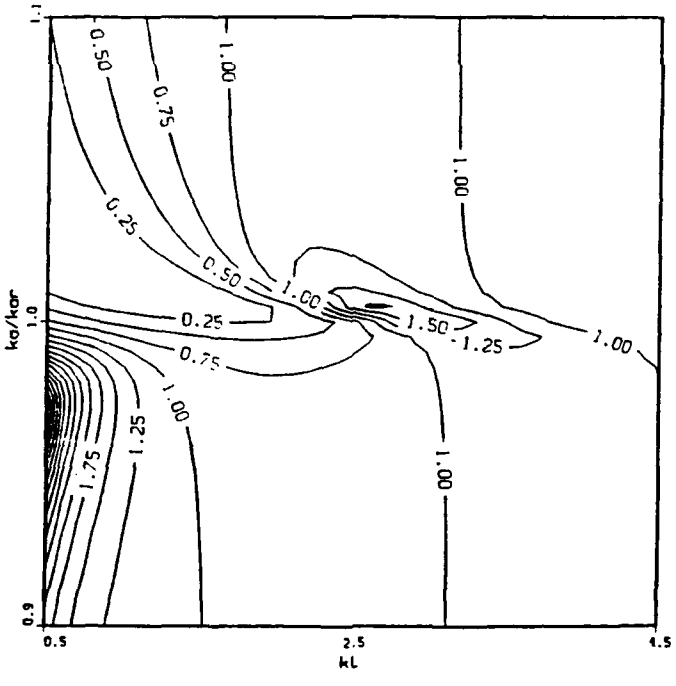

b.

Figure 3-2a,b. Surface and contour plots of G_R as a function of ka and kl_{n0} for N = 4. Planar configuration. P_0 = 1 atm.

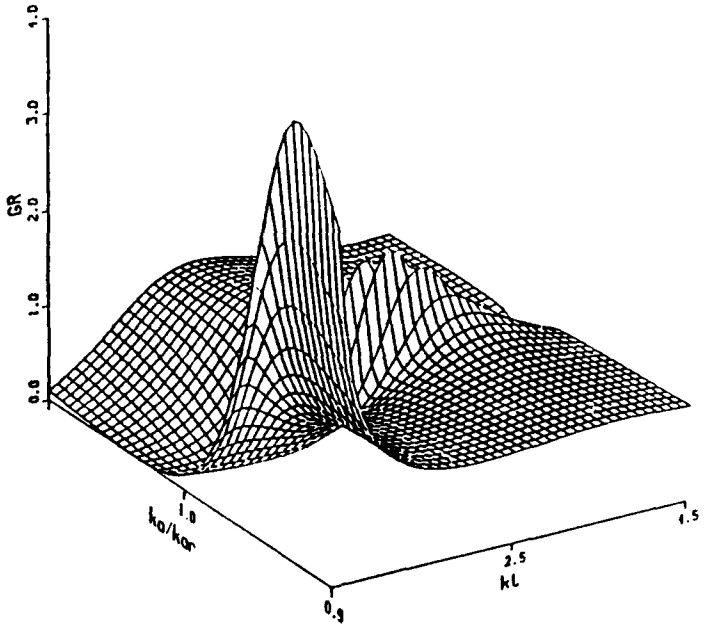

c.

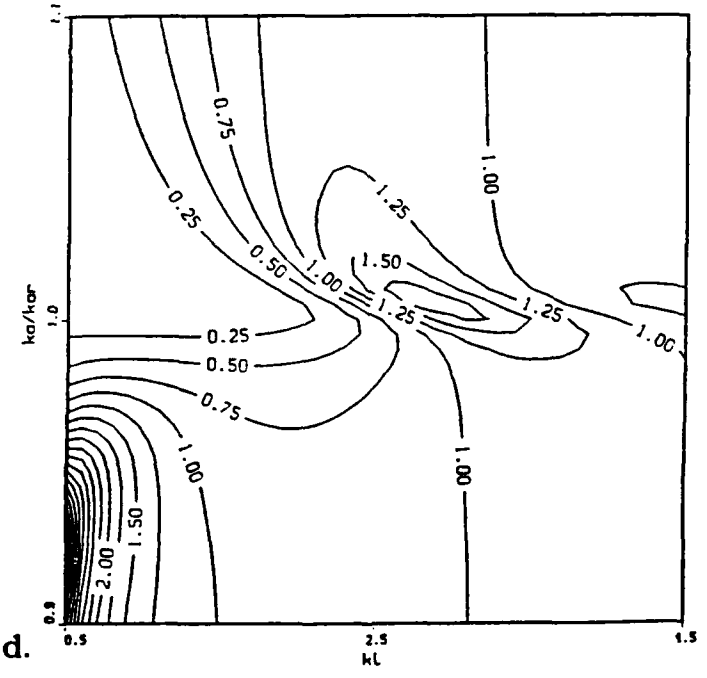

d.

Figure 3-2c,d. Surface and contour plots of G_R as a function of ka and kl_{n0} for N = 8. Planar configuration. P_0 = 1 atm.

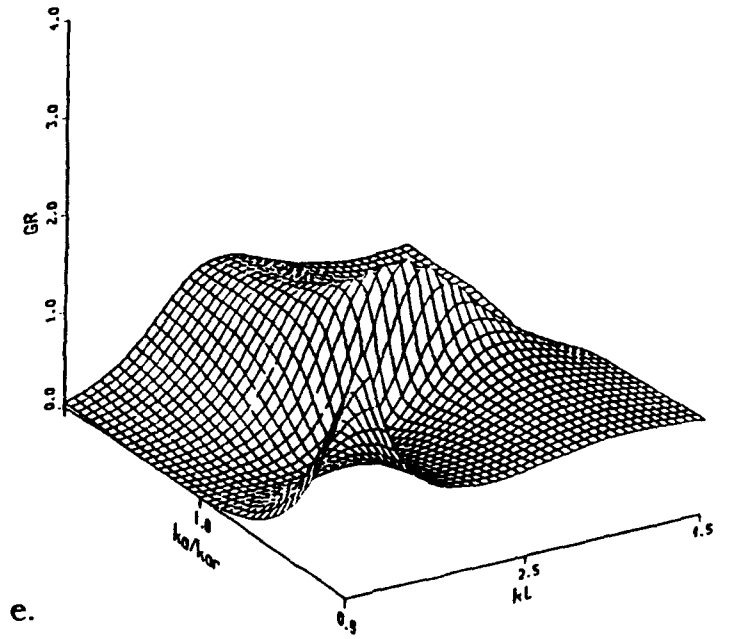

e.

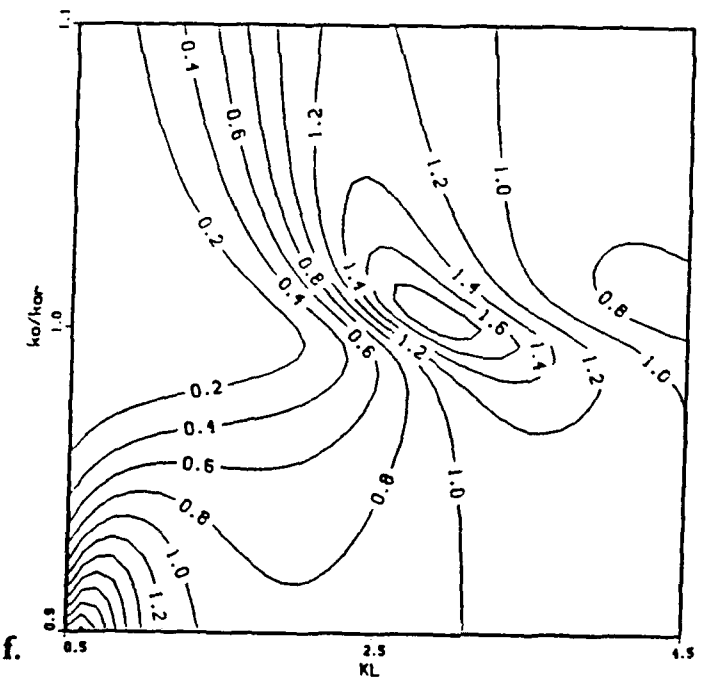

f.

Figure 3-2e,f. Surface and contour plots of G_R as a function of ka and kl_{n0} for N = 15. Planar configuration. P_0 = 1 atm.

B.1. PLANAR CONFIGURATION BEAM PATTERNS

Polar plots of the beam patterns can be developed for the planar configuration using the axis system defined in Figure 3-3. The origin is located at the transducer, with the resonators located in the x,y plane and with θ being the angle measured from the positive y axis in the x,y plane.

Figure 3-4 clearly demonstrates the acoustic advantage of the planar configuration over that of a lone transducer. The zero dB reference is taken as the field of an identical transducer with equal volume velocity, in the absence of the resonators.

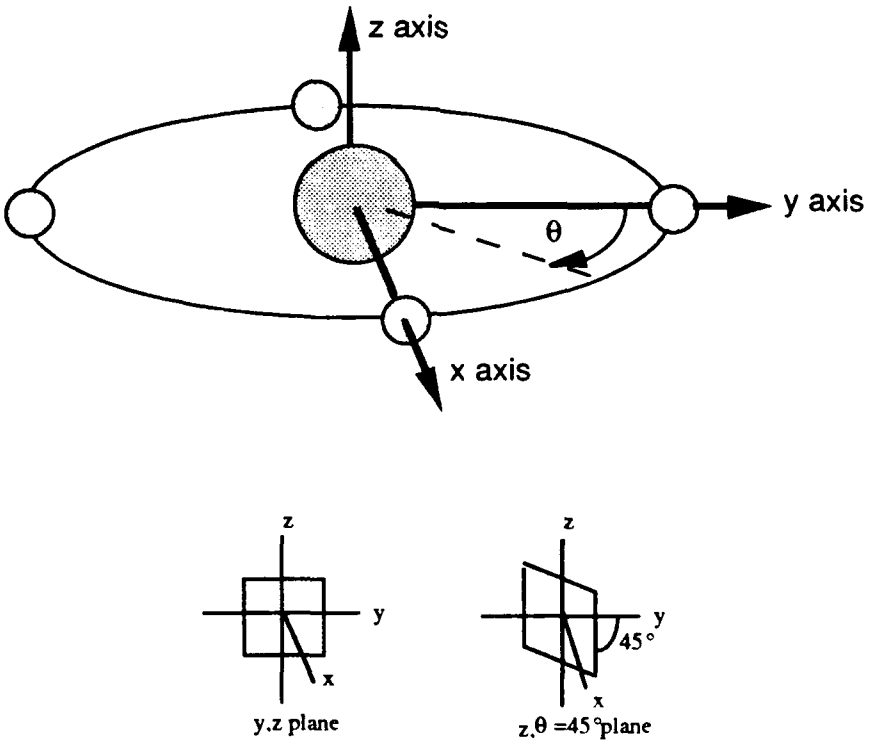

Figure 3-3. Axis system for beam patterns plots. Planar configuration. Note the definitions of the y,z and z,θ = 45° planes.

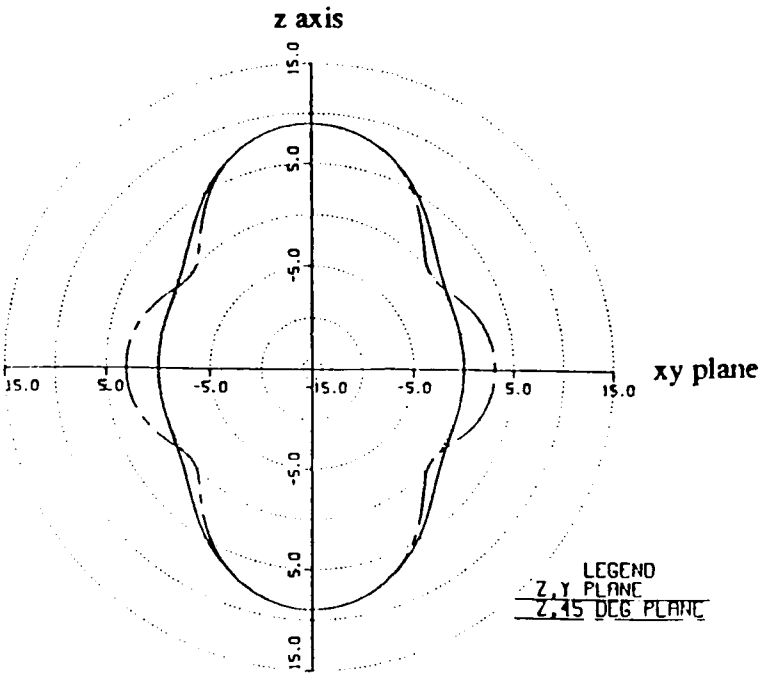

Figure 3-4. Beam patterns in the y,z and z,θ = 45° planes. Planar configuration. P_0 = 1atm. Scale in decibels (dB).

C. ANALYSIS OF CONICAL CONFIGURATION

The second geometric arrangement analyzed was chosen to take advantage of the 90° phase shift between the volume velocity of the resonators and the transducer for maximum radiated power. If the transducer is offset from the plane of the resonators by one-quarter wavelength along the positive z axis, the radiation from the resonators will constructively interfere with that of the transducer along the positive z axis. This configuration will increase the directivity of the system. This arrangement will be referred to as the conical configuration, and is shown in Figure 3-5.

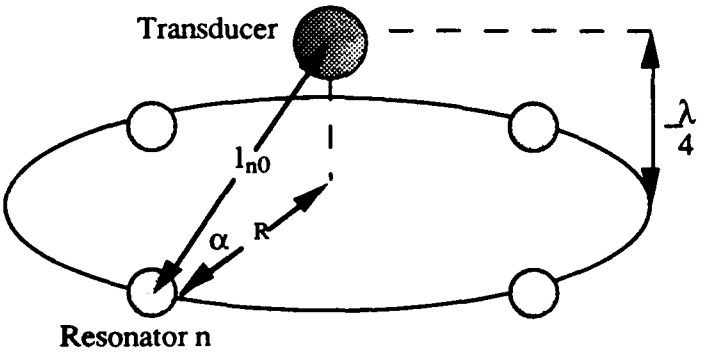

Figure 3-5. Resonators equally spaced around transducer in a conical configuration at radius R. N = 4. The transducer is displaced out of the plane of the resonators by a distance of λ/4.

The value of G_R can again be expressed in terms of ka and kl_{n0} using Equation 3-1, where Equation 3-4 is used to express kl_{nm} in terms of n, m, and kl_{n0} for the conical configuration.

$$kl_{nm} = \sqrt{(kl_{n0})^2 - \left(\frac{\pi}{2}\right)^2}\ 2\sin\left(\frac{\pi}{N}|n-m|\right);\quad n,m = 1...N. \qquad (3\text{-}4)$$

The gain in radiation resistance for the conical configuration for the cases N = 4, 8, and 15 are plotted in the form of surface and contour plots, as shown in Figures 3-6a through 6f. Inspection of these plots reveals the existence of the same local maximum as the planar configuration of magnitude slightly less than 2 at $kl_{n0} \cong \pi$ and ka ≅ 0.01379. Note that, unlike the planar case, the kl axis of Figures 3-6a through f begins at kl_{n0} = 1.75 vice 0.5. This is due to the displacement of the transducer in the positive z direction. This displacement requires kl_{n0} be at least π/2.

The local maximum values for G_R at $kl_{n0} \cong \pi$, ka ≅ 0.01379 for

various values of N ranging from 2 to 25 and their associated parameters are tabulated in Table 3-2 for the conical configuration. In each case the value of G_R for the conical configuration is slightly less than for the planar configuration. Also, the value of kl_{max} is slightly greater for the the conical configuration, but is still approximately equal to π (A value of π for kl_{n0} corresponds to a value of 30 degrees for the angle α in Figure 3-5.).

N	G_R	ka_{max}	kl_{max}	$mag(U_n^{rel})$	$arg(U_n^{rel})$
2	1.29	0.01382	2.77	0.429	90.0°
4	1.78	0.01383	3.08	0.601	90.0°
6	1.82	0.01385	3.12	0.428	90.0°
8	1.82	0.01386	3.12	0.321	90.0°
10	1.82	0.01385	3.12	0.257	90.0°
15	1.82	0.01383	3.12	0.171	90.0°
20	1.82	0.01378	3.12	0.128	90.0°
25	1.82	0.01372	3.12	0.103	90.0°

Table 3-2. Values of G_R for N ranging from 2 to 25 and the parameters associated with the local maximum at $kl \cong \pi$, $ka \cong kl_r = 0.01379$. Conical configuration.

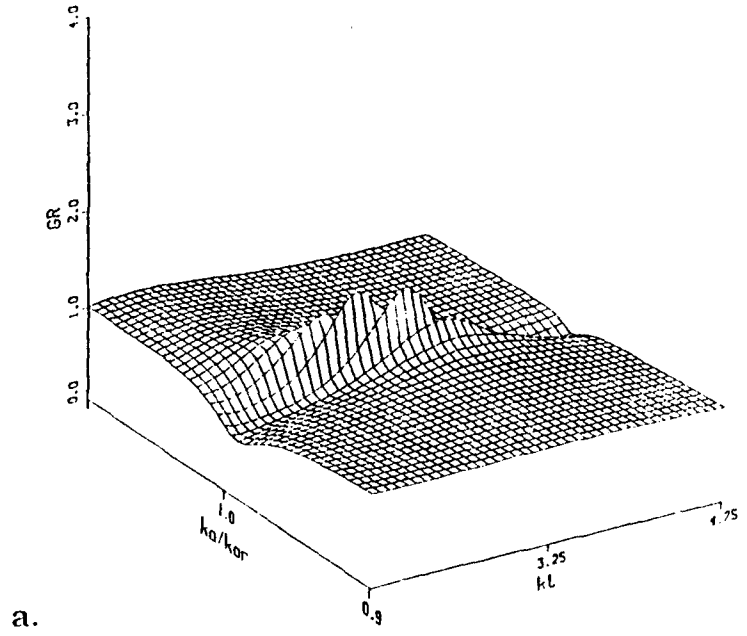

a.

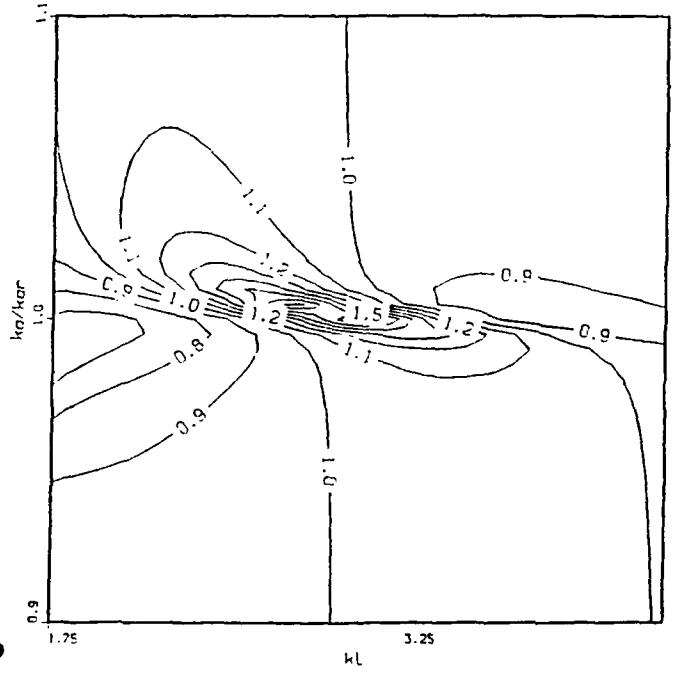

b

Figure 3-6a,b. Surface and contour plots of G_R as a function of ka and kl_{n0} for N = 4. Conical configuration. P_0 = 1 atm.

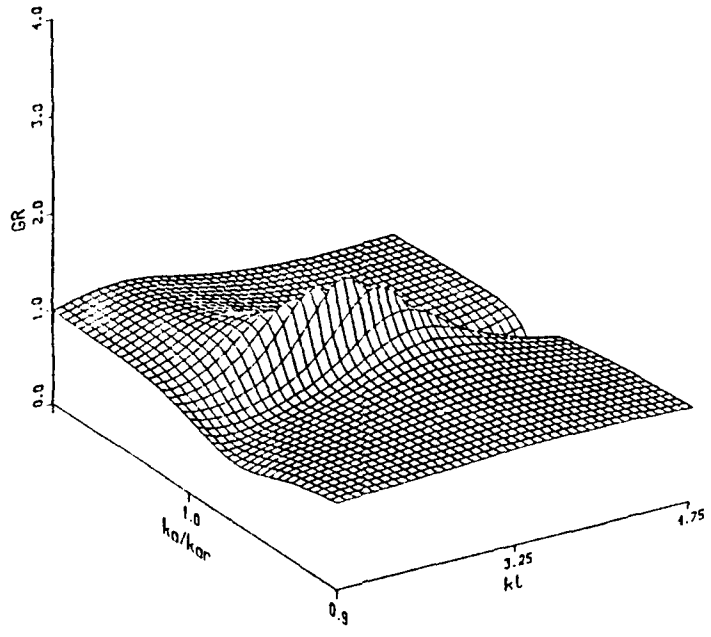

c.

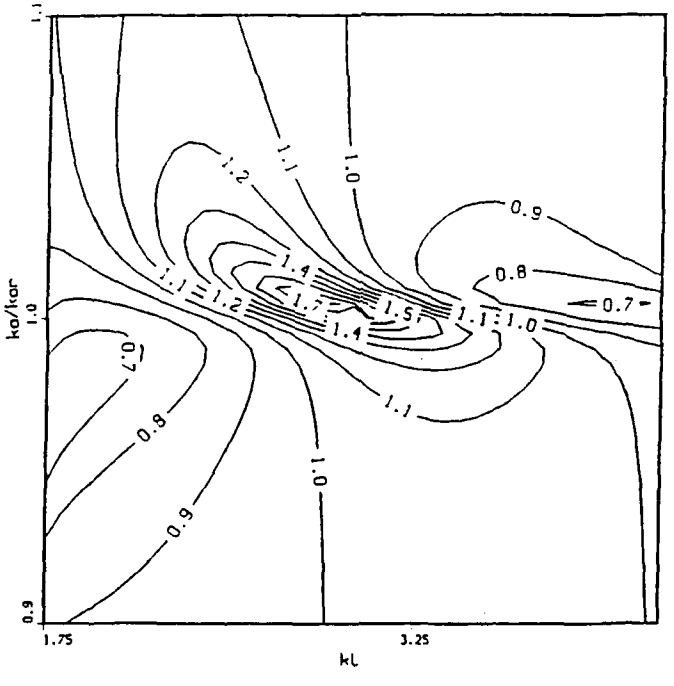

d.

Figure 3-6c,d. Surface and contour plots of G_R as a function of ka and kl_{n0} for N = 8. Conical configuration. P_0 = 1 atm.

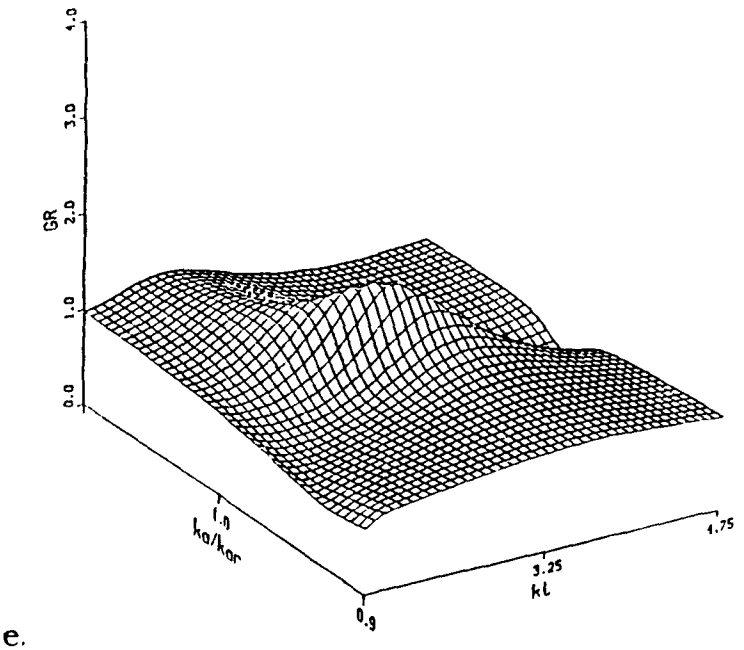

e.

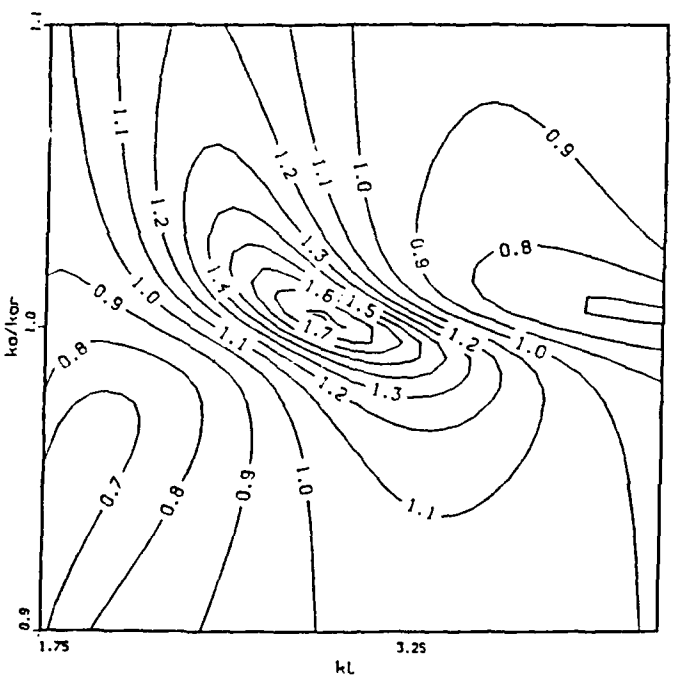

f.

Figure 3-6e,f. Surface and contour plots of G_R as a function of ka and kl_{n0} for N = 15. Conical configuration. P_0 = 1 atm.

C.1. CONICAL CONFIGURATION BEAM PATTERNS

To demonstrate the improved directivity of the conical configuration over that of the planar system, polar plots can be developed using the axis system as defined in Figure 3-7, where the transducer is displaced in the positive z direction from the plane of the resonators.

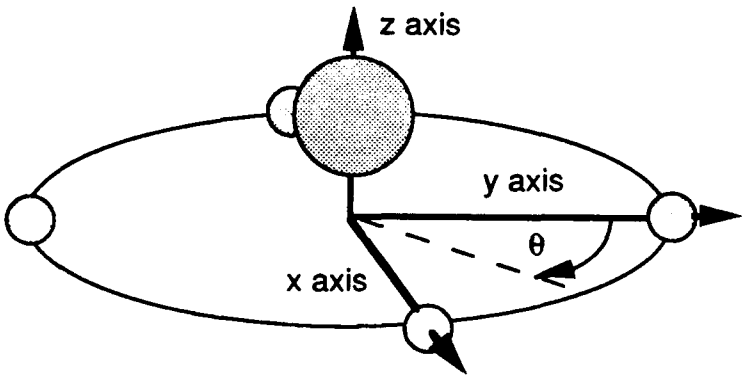

Figure 3-7. Axis system for beam pattern plots. Conical configuration.

Figure 3-8a shows the beam pattern of the conical configuration in both the y,z and the z,θ = 45° planes. As expected, the symmetry in the y,z plane about the z axis is lost, with the sound pressure level (SPL) in the positive z direction being 8 dB greater than in the negative z direction. If one compares the beam patterns of the conical configuration to that of the planar configuration, shown in Figure 3-8b, one observes that the SPL in the positive z direction for the conical configuration is 1 dB greater than for the planar configuration, and 10 dB greater than for one transducer alone. Figure 3-8b clearly shows that significant directional discrimination can be achieved with only a

minor decrease in total power gain, G_R.

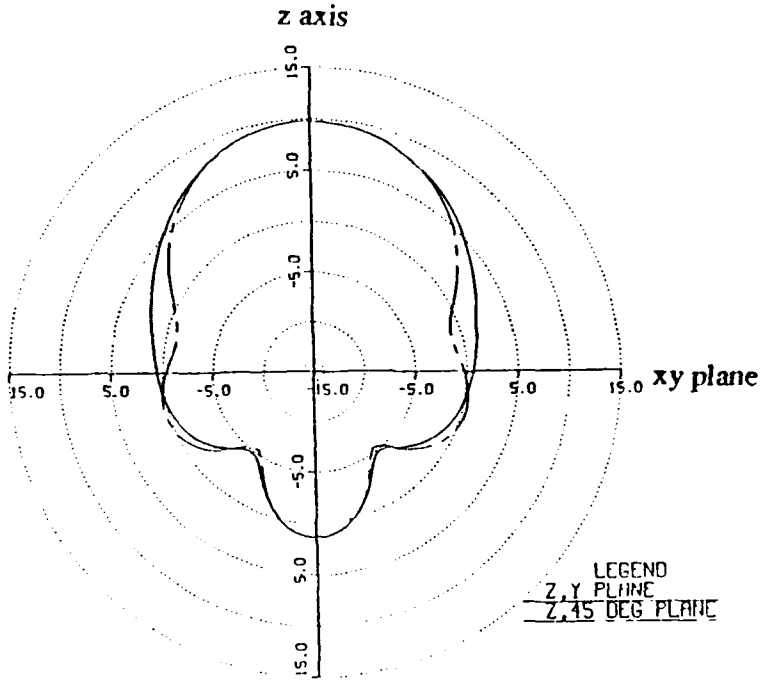

Figure 3-8a. Beam patterns in the y,z and z,θ = 45° planes. Conical configuration. P_0 = 1 atm. Scale in decibels (dB).

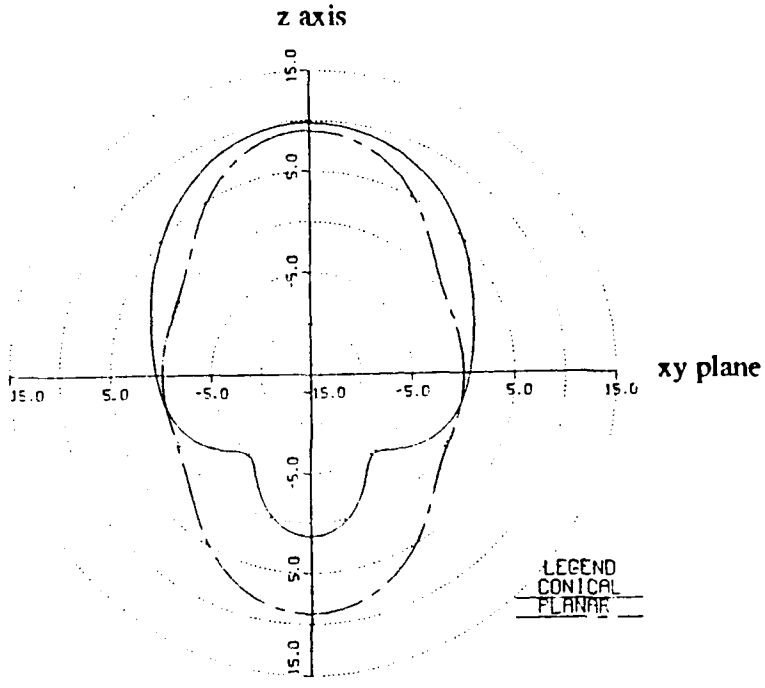

Figure 3-8b. Beam-patterns in the y,z plane for the planar and conical configurations. P_0 = 1 atm. Scale in decibels (dB).

D. OPTIMUM CONFIGURATION

The results of all calculations performed have been presented in terms of the dimensionless radius and spacing, ka and kl_{n0}. The actual dimensions for the radius a and the separation distance l_{max} for a given frequency are obtained using Equation 3-5:

$$a = \frac{kac}{2\pi f} \qquad l_{n0} = \frac{kl_{n0}c}{2\pi f} . \tag{3-5}$$

Taking $ka \cong ka_r = 0.01379$ and $kl_{n0} \cong \pi$ in Equation 3-5 for the optimum values of a typical system at an ambient pressure of one atmosphere, a plot of the resulting dimensions a and l_{n0} as a function of frequency can be made, as shown in Figures 3-9a and 3-9b:

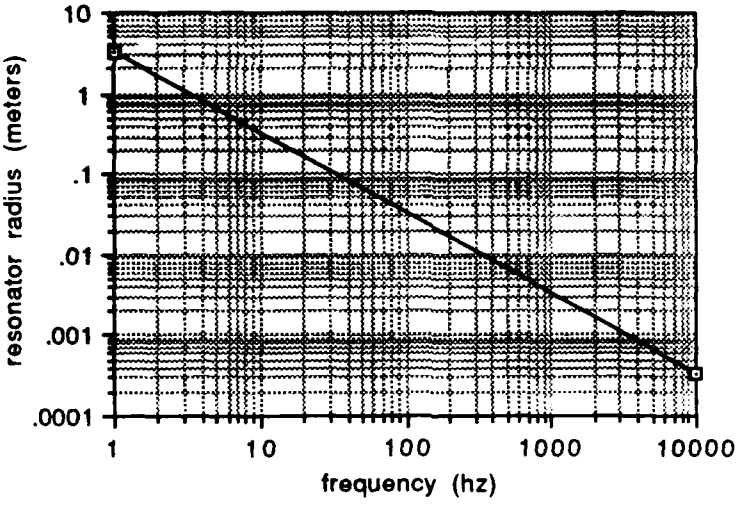

Figure 3-9a. Optimum resonator diameter (a) at resonance versus frequency. P_0 = 1 atm.

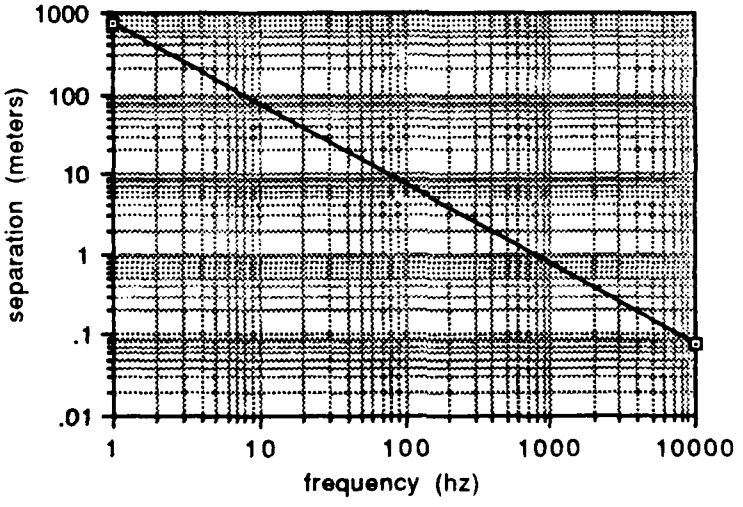

Figure 3-9b. Optimum resonator-transducer separation distance (l_{n0}) for maximum power gain versus frequency. P_0 = 1 atm.

E. ANALYSES WITH TRANSDUCER ka = CONSTANT AND P_0 = 50 ATM

Two major assumptions that have been made throughout the analysis up this point are now modified. The first is that the ambient pressure is one atmosphere and the second is that the radius of the transducer equals that of the resonators ($ka_0 = ka_n$). In the following analysis, an ambient pressure of 50 atmospheres (corresponding to a depth of 500 meters) will be taken as a more realistic value for an operational system. Since the internal acoustic impedance of a bubble is a function of depth, the value for ka_r of a single bubble at resonance will shift from 0.01379 (P_0 = 1 atm) to 0.09754 (P_0 = 50 atm). Also, the value of ka_0 will no longer be considered equal to that of the resonators, but will be held constant at various specific values.

In the previous sections it was shown that little is gained when the number of sympathetic resonators is greater than about four; hence the following analysis will be restricted to the case N = 4. Conducting similar calculations as before, contour plots and surface plots have been generated for the cases N = 4, ka_0 = 0.05, 0.10 and 0.20, for both the conical configuration (Figures 3-10a through 3-10f) and the planar configuration (Figures 3-11a through 3-11f). As in the previous analyses where the ambient pressure was taken to be one atmosphere, all cases display a local maximum of G_R of slightly less than 2 for $ka \cong ka_r = 0.09754$ and $kl \cong \pi$. These maximum values are tabulated in Table 3-3. Also tabulated, though not plotted, are the cases ka_0 = 0.025 and 0.150. The first entry in Table 3-3 for either configuration was calculated by holding ka_0 equal to ka_n, as in previous calculations, vice holding ka_0 constant. A review of Table 3-3 and Figures 3-11 and

12 demonstrates that the value of ka_0 has little effect on the achievable power gain.

configuration	ka_0	G_R	ka_{max}	kl_{max}	$mag(U_n^{rel})$	$arg(U_n^{rel})$
planar	ka_n	1.87	0.09987	2.82	0.649	90.0°
	.025	1.87	0.09987	2.82	0.652	90.0°
	.050	1.87	0.09987	2.82	0.652	90.0°
	.100	1.87	0.09987	2.82	0.649	90.0°
	.150	1.87	0.09987	2.82	0.645	90.0°
	.200	1.87	0.09998	2.82	0.639	90.0°
conical	ka_n	1.78	0.09990	3.08	0.601	90.0°
	.025	1.78	0.09990	3.08	0.603	90.0°
	.050	1.78	0.09990	3.08	0.603	90.0°
	.100	1.78	0.09990	3.08	0.601	90.0°
	.150	1.78	0.09990	3.08	0.597	90.0°
	.200	1.78	0.09990	3.08	0.592	90.0°

Table 3-3. Values of G_R for various values of ka_0 ranging from 0.025 to 0.2 and the parameters associated with the local maximum at $kl \cong \pi$, $ka \cong ka_r = 0.09754$. Conical and planar configurations. $P_0 = 50$ atm.

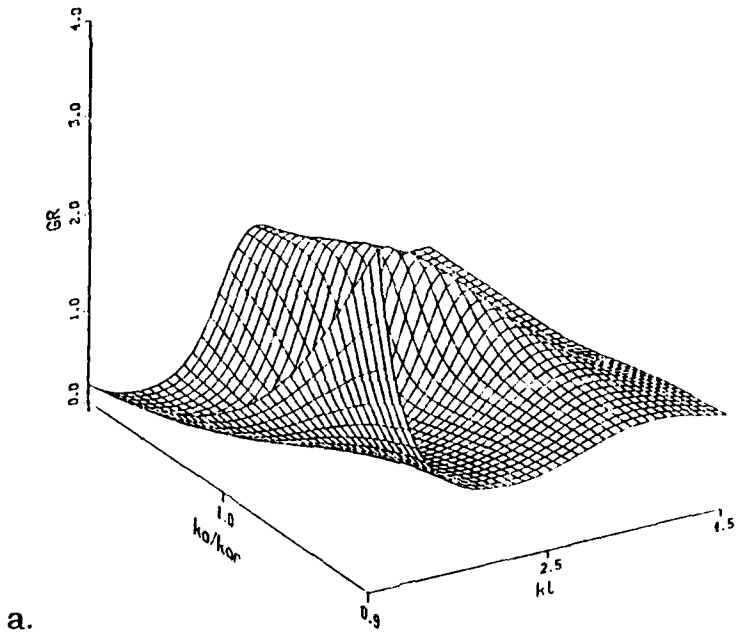

a.

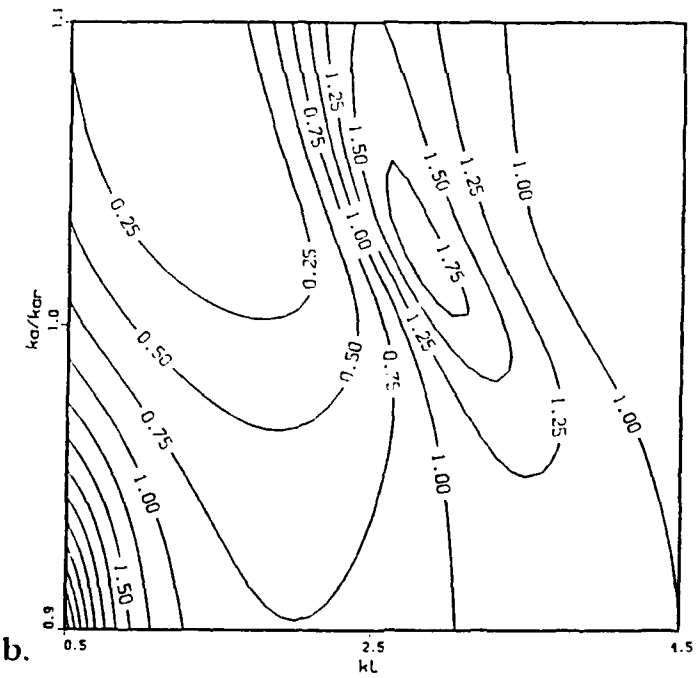

b.

Figure 3-10a,b. Surface and contour plots of G_R as a function of ka and kl_{n0} for N = 4. Planar configuration. P_0 = 50 atm. ka_0 = 0.05.

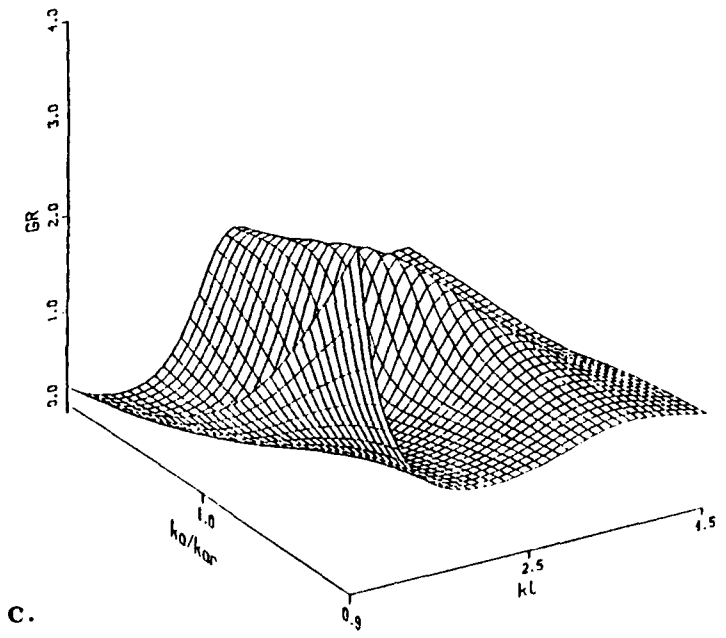

c.

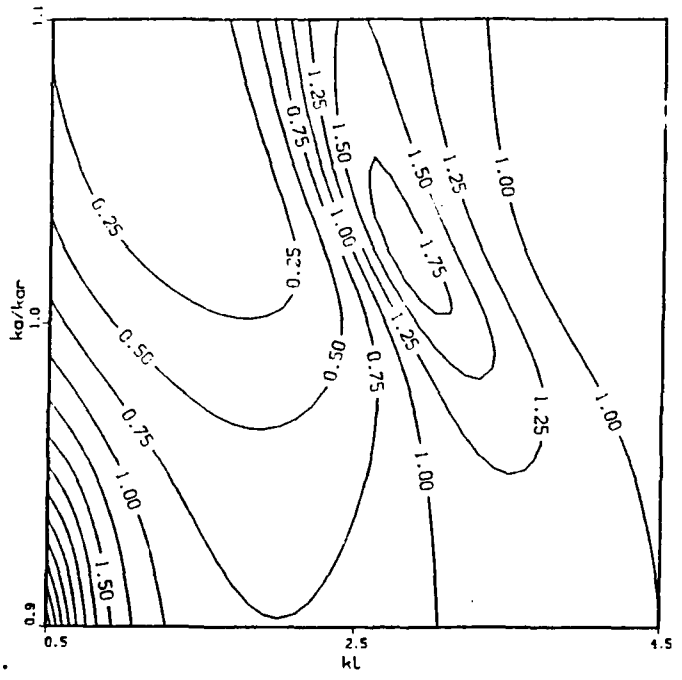

d.

Figure 3-10c,d. Surface and contour plots of G_R as a function of ka and kl_{n0} for N = 4. Planar configuration. P_0 = 50 atm. ka_0 = 0.10.

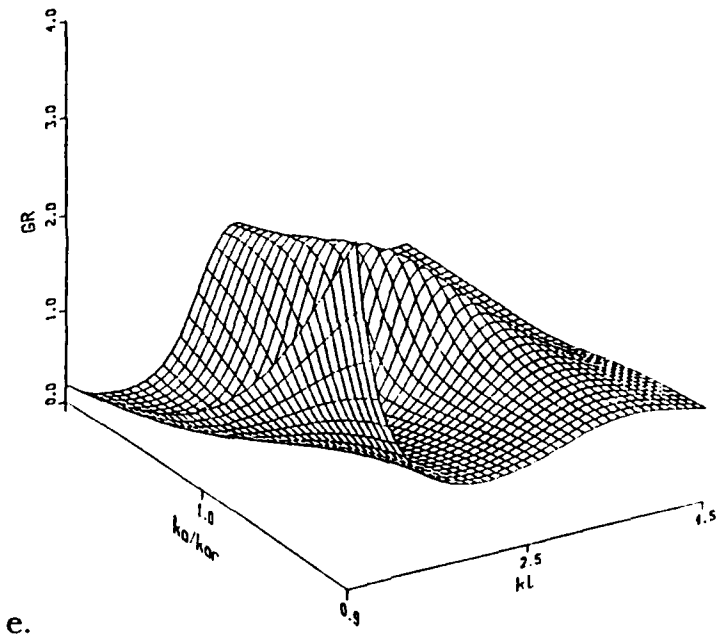

e.

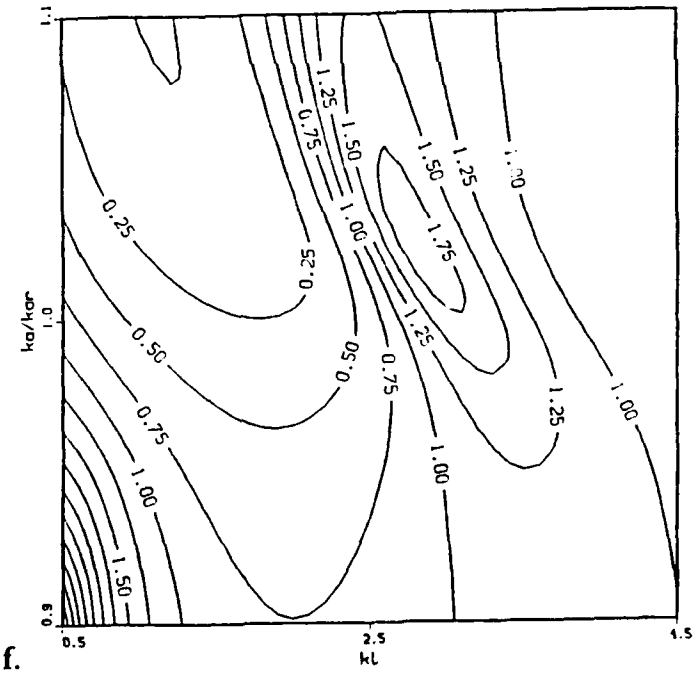

f.

Figure 3-10e,f. Surface and contour plots of G_R as a function of ka and kl_{n0} for N = 4. Planar configuration. P_0 = 50 atm. ka_0 = 0.20.

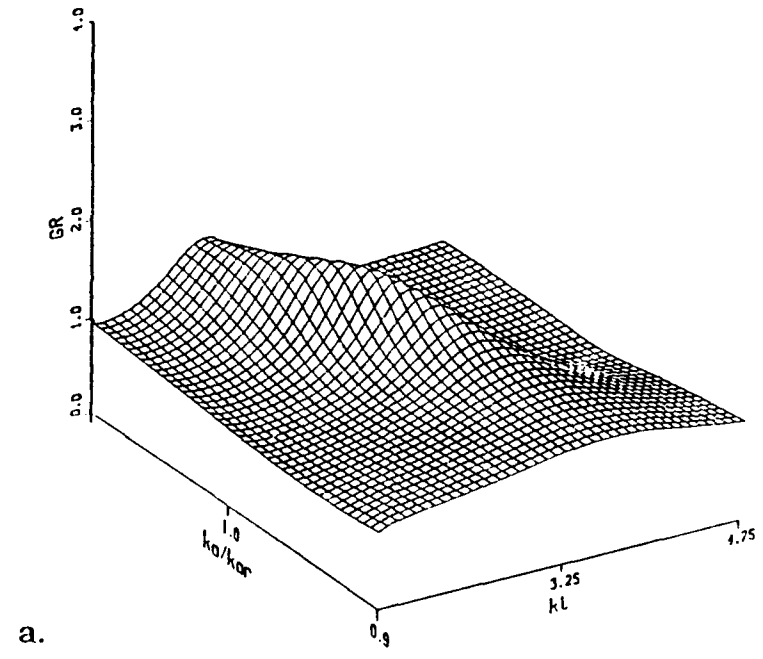

a.

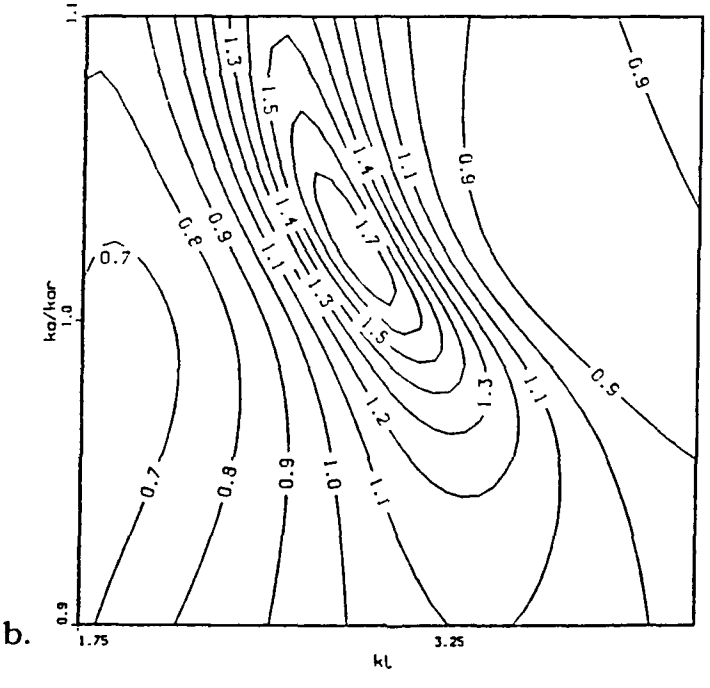

b.

Figure 3-11a,b. Surface and contour plots of G_R as a function of ka and kl_{n0} for N = 4. Conical configuration. P_0 = 50 atm. ka_0 = 0.05.

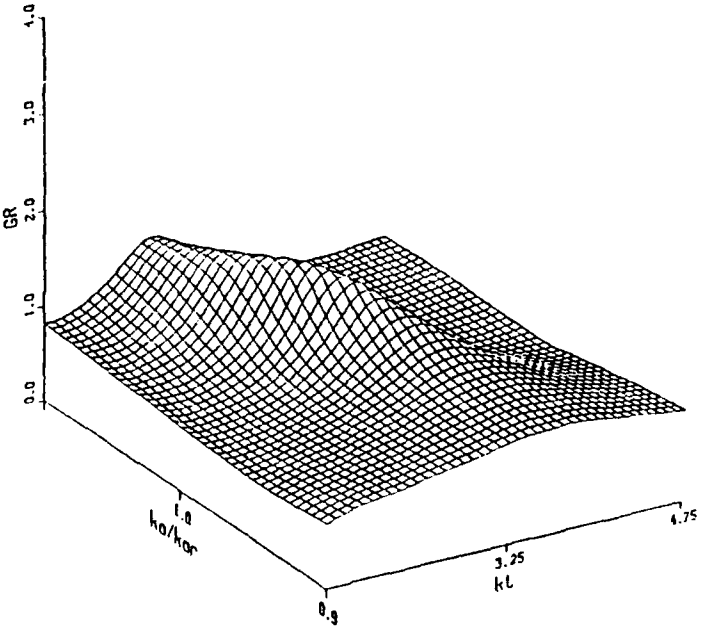

c.

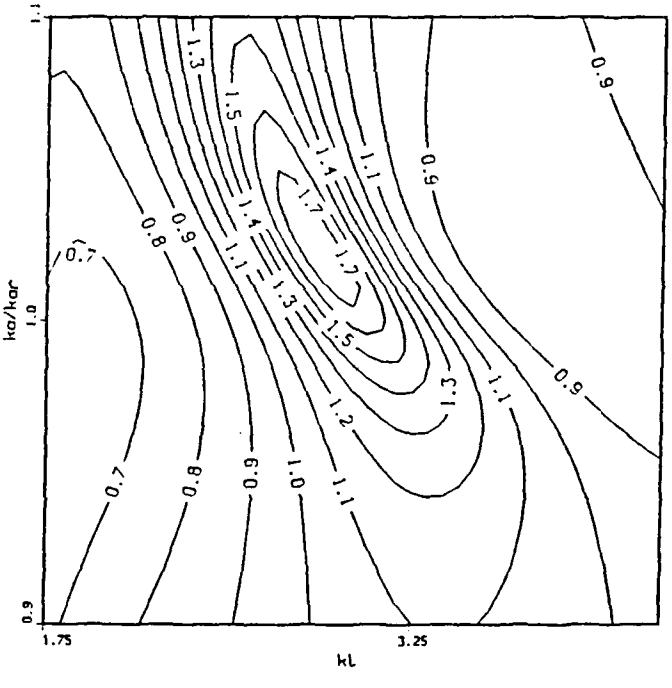

d.

Figure 3-11c,d. Surface and contour plots of G_R as a function of ka and kl_{n0} for N = 4. Conical configuration. P_0 = 50 atm. ka_0 = 0.10.

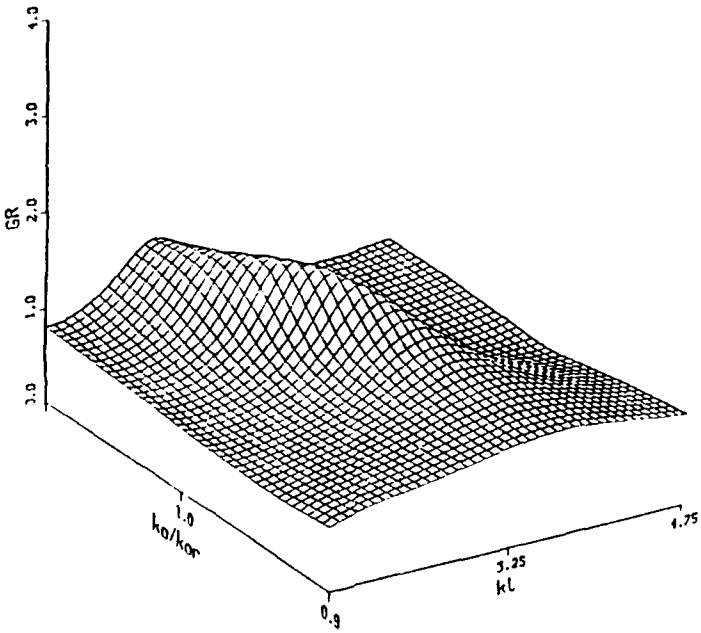

e.

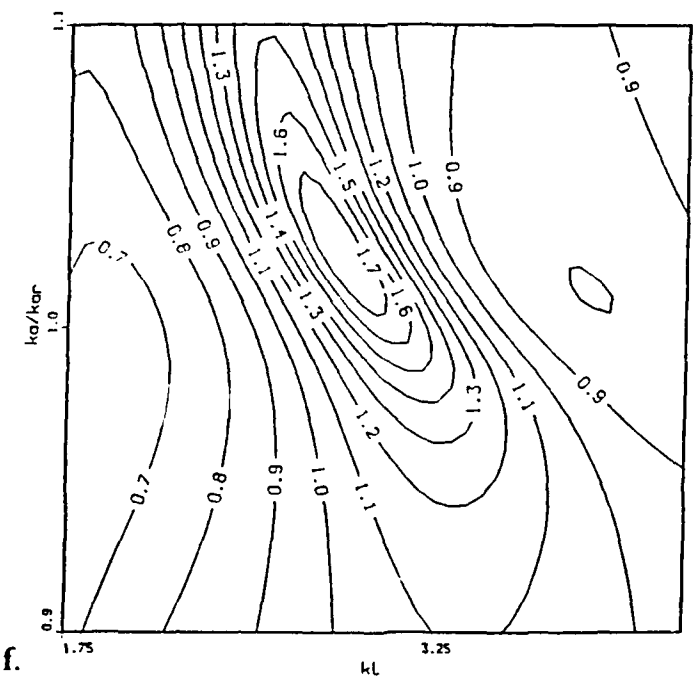

f.

Figure 3-11e,f. Surface and contour plots of G_R as a function of ka and kl_{n0} for N = 4. Conical configuration. P_0 = 50 atm. ka_0 = 0.20.

E.1. BEAM PATTERNS, P_0 = 50 ATM

Since there is no significant variation in gain with the value of ka_0, beam patterns were only developed for the case $ka_0 = ka_r$, and are shown in Figures 3-12 through 3-14. These plots show the maximum SPL in the positive z direction for the conical configuration to be 1.5 dB greater than for the planar case and 10.5 dB greater than for the transducer in the absence of the resonators.

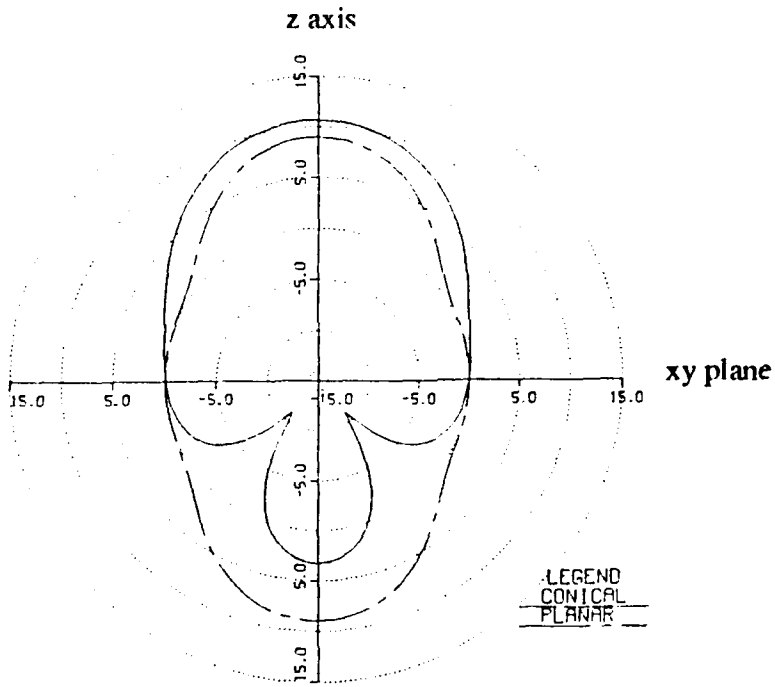

Figure 3-12. Beam patterns in the y,z plane for the planar and conical configurations. P_0 = 50 atm. Scale in decibels (dB).

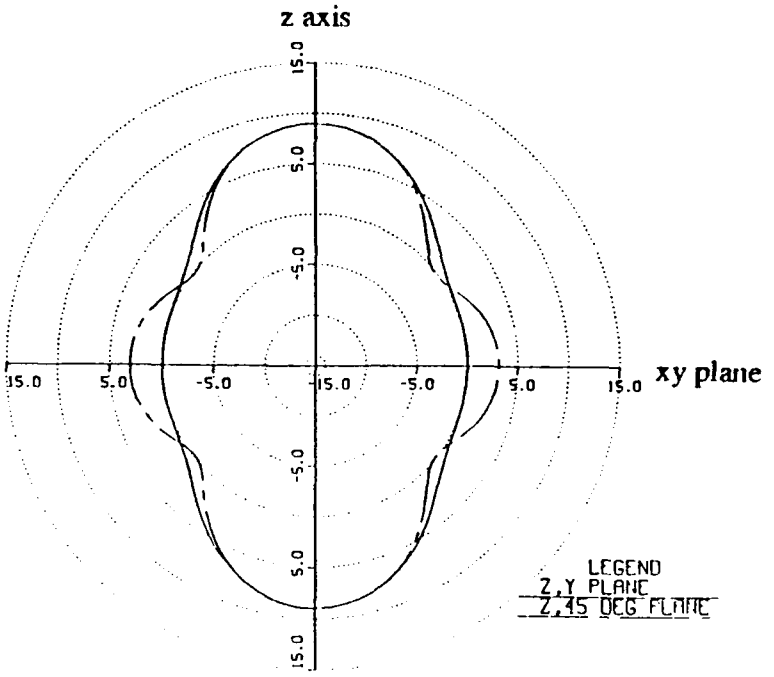

Figure 3-13. Beam patterns in the y,z and z,θ = 45° planes. Planar configuration. P_0 = 50 atm. Scale in decibels (dB).

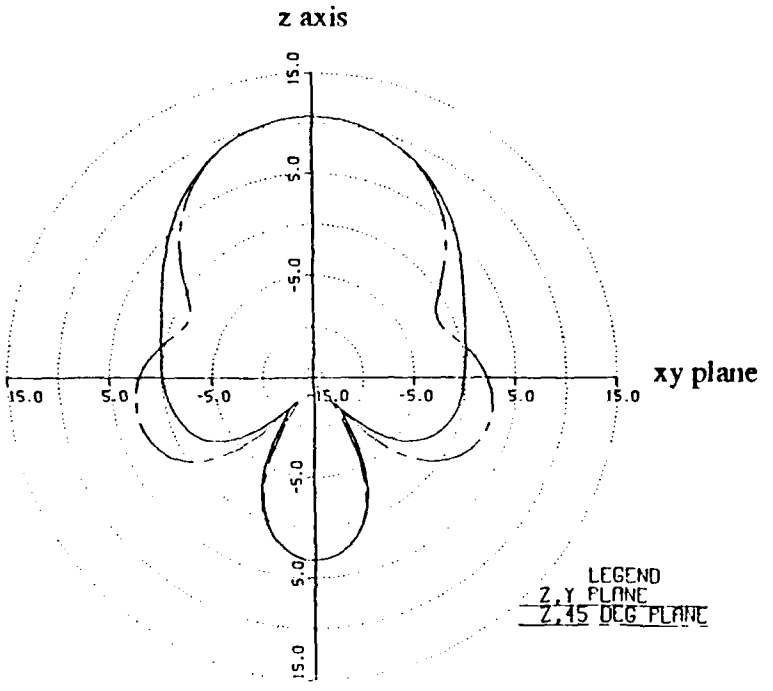

Figure 3-14. Beam patterns in the y,z and z,θ = 45° planes. Conical configuration. P_0 = 50 atm. Scale in decibels (dB).

E.2. OPTIMUM CONFIGURATION, P_0 = 50 ATM

The actual dimensions of the resonator radius a and the separation distances l_{n0}, for a system operated at an ambient pressure of 50 atmospheres, were calculated using Equation 3-5 using the optimum values $ka \cong ka_r = 0.09754$ and $kl_{n0} \cong \pi$. Since the values of l_{n0} are not depth-dependent, Figure 3-9b still applies. Figure 3-15 displays the relation between the optimum resonator radius and frequency for an ambient pressure of 50 atmospheres.

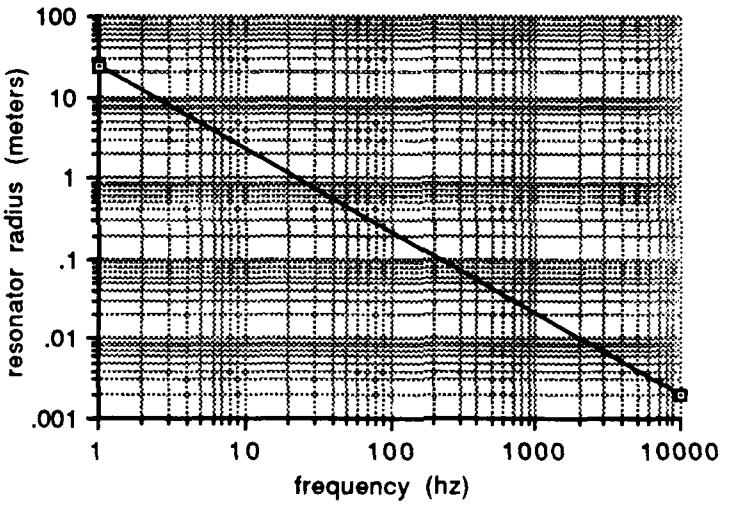

Figure 3-15. Optimum resonator diameter (a) at resonance verses frequency. P_0 = 50 atm.

IV. SUMMARY, CONCLUSIONS AND RECOMMENDATIONS

A. SUMMARY

The problem of multiple-scattering of an incident plane-wave from a system of compact resonant-scatterers was solved using both Tolstoy's method and network analysis. It was shown that these two methods of analysis are equivalent and that both predict the existence of "quasiresonance". Network analysis was then applied to a circular array of scatterers, where the incident plane-wave was replaced by spherical waves radiated from an active transducer, located on the center axis. The acoustic advantage of this system was quantified by the gain in the radiation resistance seen by the transducer in the presence of these scatterers compared to a lone transducer. Two configurations were analyzed: (1) the transducer in the plane of the resonators, and (2) the transducer displaced by one-quarter wavelength from the plane. Both configurations showed a gain in radiation resistance of almost a factor of two and an improved directivity over that of a single transducer.

B. CONCLUSIONS

The numerical analysis of a transducer surrounded by a circular array of sympathetic resonators indicates that a gain in radiation resistance of about two is obtainable compared to a lone transducer. The physical dimensions of such a system operating at an ambient pressure of 50 atmospheres are displayed in Table 4-1 for several frequencies of interest.

Frequency (Hz)	Resonator Radius (a) (m)	System Radius (R) (m)	
		conical	planar
10	0.329	64.9	74.9
100	0.0329	6.49	7.49
1000	0.00329	0.649	0.749

Table 4-1. Dimensions of planar and conical configurations for various frequencies. P_0 = 50 atm. R is the radius of the array.

Although the calculations presented here were for spherical bubbles, the results also apply to more realistic devices (e.g. thin shelled cavities, balloons, etc) as long as they are compact (ka << 1). M. Strasberg [Ref. 6] showed that the shape of a resonant body has little effect on its fundamental resonance frequency. For example, he calculated that an oblate spheroid with a ratio of lengths of major to minor axes of four, the fundamental resonance frequency differs by only a factor of 1.08 from that of a sphere with the same volume. Therefore, any deformation of the resonators from a true spherical shape, for example due to forces such as buoyancy, should have little affect on system performance.

C. RECOMMENDATIONS

The results of the research reported in this thesis are very encouraging. It is recommended that follow-on work include the design, construction, and testing of an array to verify the theoretical predictions presented.

Theoretical analysis remains to be conducted in at least four areas.

First, in all of the calculations performed, the sympathetic resonators were assumed to be gas-filled air bubbles executing radial oscillations only. A more realistic model of a sympathetic resonator may be required, based upon the properties of a practical device. It is recommended this be investigated. Second, Tolstoy has shown that the scattering of an incident plane-wave from a linear array of resonant scatterers exhibits strong directionality. Perhaps a linear array of sympathetic resonators offers better performance gain than the circular arrays considered in this research. It is recommended that such a configuration be investigated. Third, it was shown that in the optimum conical configuration the ring of sympathetic resonators lies on a cone with a apex angle of approximately 120 degrees, independent of frequency. This suggests that a broad-band, constant directivity system could be constructed using a series of concentric rings of resonators, each tuned to a slightly different frequency and placed in its appropriate location along the surface of such a cone, as indicated in Figure 4-1. It is recommended that the properties of such a system be investigated. Fourth, in the calculations presented, the sympathetic resonators were all assumed to be identical, and their locations were assumed to be precisely known, as well as that of the transducer. It is recommended that the effects of resonator nonuniformity and imprecise location be investigated.

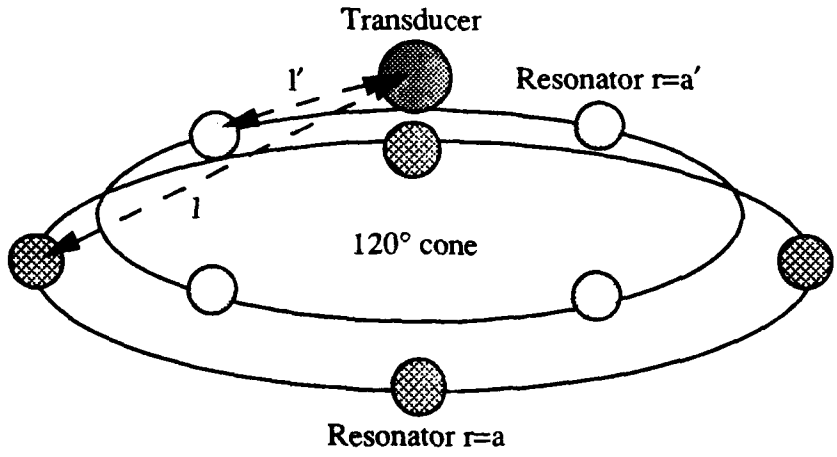

Figure 4-1. Multiple-ring conical configuration allowing an expanded frequency response. Two concentric rings of resonators of radii a and a', separated from the transducer by distances of l and l', respectively.

REFERENCES

[1] Tolstoy, I., "Superresonant Systems of Scatterers. I," J. Acoust. Soc. Am. **80**, 282-294 (1986).

[2] Tolstoy, I., "Erratum: Superresonant Systems of Scatterers. I," [J. Acoust. Soc. Am. **80**, 282-294 (1986)], J. Acoust. Soc. Am. **81**, 1987 (1987).

[3] Tolstoy, A. and Tolstoy I., "Superresonant Systems of Scatterers. II," J. Acoust. Soc. Am. **83**, 2086-2096 (1988).

[4] Tolstoy, I., "Resonance and Directionality of Linear Arrays of Monopole Scatterers.," J. Acoust. Soc. Am. **84 S1**, S218 (1988).

[5] Kinsler, L. E., Frey, A. R., Coppens, A. B., and Sanders, J. V., *Fundamentals of Acoustics, Third Edition*, John Wiley & Sons, Inc., 1982, pp. 228-231.

[6] Strasberg, M., "The Pulsation Frequency of Nonspherical Gas Bubbles in Liquids," J. Acoust. Soc. Am. **25**, 536-537 (1953).

BIBLIOGRAPHY

Kinsler, L. E., Frey, A. R., Coppens, A. B., and Sanders, J. V., *Fundamentals of Acoustics, Third Edition*, John Wiley & Sons, Inc., 1982.

Clay, C. S., and Medwin H., *Acoustical Oceanography*, John Wiley & Sons, Inc., 1977.

LIST OF SYMBOLS

a_n	Radius of element n.
c	Speed of sound in water.
G_R	The ratio of the acoustic radiation resistance of a transducer with sympathetic resonators present to the acoustic radiation resistance of an identical transducer with no resonators present.
k	Wave number, ω/c.
ka_r	The resonance value of ka for a single air-filled bubble.
l_{nm}	Separation distance between element n and m.
p_n^f	Incident free field acoustic pressure at element n due to external field only.
p_n	Surface pressure at element n.
p_n^{sc}	Scattered pressure at the surface of resonator n, in the presence of other resonators.
p_{single}^{sc}	Scattered pressure at the surface of a single resonator. i.e. in the absence of other resonators.
r	Distance from scatterer center to a field point.
z	Specific acoustic impedance, pressure divided by surface normal velocity.
A	Single-scattering amplification coefficient of element n.
B	Multiple-scattering amplification coefficient of element n.
C_{nm}	Ratio of acoustic impedances, defined as: $C_{nm} = \frac{Z_{nm}^{ar}}{Z_{mm}^{ar}}$.
D_n	Ratio of acoustic impedances, defined as: $D_n = -\frac{Z_{nn}^{ar} + Z_n^a}{Z_{nn}^{ar}}$.

F_a Scattered acoustic pressure from a single scatterer, normalized to the incident acoustic field.

F_b Scattered acoustic pressure from a scatterer,interacting with other scatterers, normalized to the incident acoustic field

I Electrical current.

P_0 Ambient pressure of environment.

S_n Surface area of element n.

T Transduction coefficient.

U_n Volume velocity of element n.

U_n^{rel} Volume velocity of element n, normalized to transducer volume velocity.

Z Acoustic impedance, pressure divided by volume velocity.

Z_n^a Acoustic impedance of element n.

Z_{nn}^{ar} Acoustic radiation impedance seen by element n with all other elements blocked.

Z_{nm}^{ar} Acoustic transfer impedance from element m to element n.

Z_{tot}^{ar} The total acoustic radiation impedance seen by transducer in the presence of sympathetic resonators.

Z^{ao} Transducer open circuit (I=0) acoustical impedance.

δ_{nm} Kronecker delta function, where: $\delta_{nm} = \begin{cases} 1; & m = n \\ 0; & m \neq n \end{cases}$.

ρ Density of water.

μ Ratio of the magnitudes of the scattered acoustic pressure at the surface of a resonant scatterer to the incident acoustic pressure in the presence of other scatterers.

μ_0 Ratio of the magnitudes of the scattered acoustic pressure at the surface of a single resonant scattererto the incident acoustic pressure.

γ Ratio of specific heats (air).

ω Angular frequency of plane wave.

ω_0 Angular frequency of scatterer resonance.

ζ Defined as: $\zeta = \dfrac{(\omega_0^2/\omega^2 - 1)}{ka}$.

$|X_n|$ A Nx1 column matrix, n = 1...N.

$[X_{nm}]$ A NxN square matrix, n,m = 1...N.